In situ Sr isotope compositions of plagioclase from a complete stratigraphic profile of the Bushveld Complex, South Africa: Evidence for extensive magma mixing and percolation

Bartosz T. Karykowski*[1], Sheng-Hong Yang[2], Wolfgang D. Maier[1], Yann Lahaye[3], C. Johan Lissenberg[1], Hugh O'Brien[3]

[1]*School of Earth and Ocean Sciences, Cardiff University, Main Building, Park Place, Cardiff CF10 3AT, UK.*

[2]*Department of Geosciences, University of Oulu, P. O. Box 3000, 90010 Oulu, Finland*

[3]*Geological Survey of Finland, Espoo, Finland*

(*corresponding author: E-Mail: KarykowskiBT@cardiff.ac.uk)

ABSTRACT

The cumulates of the Bushveld Complex, forming the largest layered intrusion on Earth, are known to have crystallised from several isotopically distinct magma pulses. Here, we present *in situ* Sr isotope compositions combined with the corresponding mineral chemistry of plagioclase from all lithological zones, covering > 6 km of stratigraphy to constrain the petrogenesis of the complex.

The *in situ* data coupled with high-resolution elemental maps of individual plagioclase grains reveal complex zonation patterns with respect to mineral chemistry and Sr isotope composition. This suggests that interstitial plagioclase in the Bushveld Complex crystallised from multiple isotopically distinct influxes of melt, percolating through a mafic cumulate framework and displacing the resident melt. Similarly, cumulus plagioclase grains are the result of continual ingress of distinct magma, which picked up previously formed plagioclase crystals.

Sr isotope compositions across the layered sequence seem to be largely decoupled from fractionation indices, such as Mg#, anorthite content or trace element ratios. As these observations cannot be explained by bulk assimilation, we propose that the elevated Sr isotopic signature of the Bushveld cumulates may have resulted from the interaction of the parental magma with a fluid derived from the up to 2-km-thick dolomitic footwall, which caused a major shift in Sr isotope composition without significantly affecting the degree of fractionation or trace element signature. The decarbonation and/or assimilation of dolomite during the intrusion of the Bushveld Complex may be of major importance not only for the petrogenesis, but also for the emplacement of the layered intrusion as devolatilisation is directly linked to space creation due to volume loss, thus producing a lopolith.

INTRODUCTION

Recent technical developments in the analysis of radiogenic isotope ratios allowed for the progression from powdered whole rock-based isotope measurements to the *in situ* isotope analysis at the single-crystal and sub-grain scale (e.g., Ramos *et al.*, 2004, 2005; Charlier *et al.*, 2006; Müller *et al.*, 2000, 2002). A number of *in situ* isotope studies on magmatic rock samples have shown that single grains may exhibit primary isotopic heterogeneity, even at the sub-grain scale (e.g., Charlier *et al.*, 2007; Davidson *et al.*, 1998; Chadwick *et al.*, 2007). As radiogenic isotope ratios remain unaffected by melting and crystallisation, they can be used as a powerful petrogenetic tool for tracing source contributions in a given magmatic succession (e.g., Faure, 1986). This provides a unique opportunity to study magmatic processes operational during an open-system magma chamber evolution (e.g., Gagnevin *et al.*, 2005; Davidson *et al.*, 2007; Gao *et al.*, 2015; Ginibre & Davidson, 2014). For example, Sr-Nd isotope disequilibrium between clinopyroxene and plagioclase in samples from the Xiaohaizi layered intrusion in NW China suggests the crystallisation of these minerals from geochemically distinct magmas (Wei *et al.*, 2014). Moreover, disequilibrium Sr isotope compositions of plagioclase within single thin sections from the Baima layered intrusion in SW China were interpreted to result from the co-accumulation of cumulus plagioclase that had crystallised from different magmas (Liu *et al.*, 2014). On the basis of Sr isotopic zoning in single plagioclase crystals from the Rum layered intrusion in Scotland, Tepley & Davidson (2003) were able to elucidate the events during crystal growth in a magma undergoing contamination.

As the largest layered intrusion on Earth, the Bushveld Complex has traditionally received considerable attention from the isotope community (Cawthorn, 2015 and references therein). Early Sr isotope studies on powdered whole rock samples and mineral separates by Eales *et al.* (1990b), Kruger & Marsh, (1982), Kruger (1990), Lee & Butcher, (1990) and

Sharpe, (1985) have provided a large body of isotope data across the Bushveld Complex, which have been complemented and synthesised by Kruger (1994). Distinct shifts in Sr isotope compositions have been identified across the layered sequence of the complex. These variations subsequently served as a basis for Kruger's (1994) subdivision of the Bushveld Complex into several zones, broadly reflecting distinct parental magma compositions. Further, Eales *et al.* (1990a) recognised Sr isotope disequilibrium between plagioclase and coexisting orthopyroxene in some samples from the Upper Critical Zone of the western Bushveld. Similar results were also reported by Roelofse & Ashwal (2012) for the lower Main Zone of the northern Bushveld. Moreover, Sr isotope compositions of plagioclase separates from the Merensky and Bastard Cyclic Units in the eastern Bushveld, analysed by Seabrook *et al.* (2005), show typical Main Zone Sr isotopic signatures. Harmer *et al.* (1995) conducted the first systematic Pb isotope study across the Bushveld Complex, concluding that Pb isotopes vary systematically in a similar manner to Sr isotope ratios. However, later studies by Mathez & Waight (2003) and Mathez & Kent (2007) also showed Pb isotope disequilibrium between different plagioclase populations as well as between coexisting plagioclase and sulfide. Disequilibrium Nd isotope compositions between plagioclase and orthopyroxene have been reported by Prevec *et al.* (2005). These authors argued that orthopyroxene crystallised early on from a contaminated magma, whereas plagioclase was subsequently derived from a relatively uncontaminated magma.

The first *in situ* study of Sr isotope compositions in the Bushveld Complex was conducted by Chutas *et al.* (2012) using a microdrilling technique. This method confirmed previous results of Sr isotope disequilibrium between coexisting plagioclase and orthopyroxene in the Critical Zone of the eastern Bushveld. Moreover, the authors recognised disequilibrium between orthopyroxenes from the Lower Zone. Yang *et al.* (2013) were the first to produce *in situ* Sr isotope data for Bushveld plagioclase using LA-MC-ICP-MS. Their study focused on

samples from the Upper Critical Zone of the western Bushveld. Disequilibrium between plagioclase rims and cores, and between cores of different plagioclase grains in a single sample was reported. These results were interpreted to reflect the co-accumulation of plagioclase grains from different parental magmas followed by further crystal growth in a residual liquid, infiltrating from other portions of the cumulate pile. The study demonstrated that the method is capable of effectively tracing the lineage of individual plagioclase crystals in a sample. More recently, Roelofse *et al.* (2015) and Mangwegape *et al.* (2016) also produced *in situ* plagioclase Sr isotope data for the Main and Upper zones of the northern Bushveld. The latter authors followed Kruger's (1994) two-stage model, arguing that the upper part of the Main Zone and the Upper Zone formed primarily in response to normal fractionation, whereas the lower part of the Main Zone originated from the repeated influx of magmas. Based on isotope disequilibrium between and within co-existing cumulus minerals, Roelofse *et al.* (2015) suggested that these influxes were essentially variably contaminated crystal mushes.

The observation of Sr isotope disequilibrium has important implications for the formation of the sampled lithology, and, by extension, for the complex as a whole. Particularly in samples from stratigraphic levels where influxes of geochemically distinct magma are known, mineral-scale isotope analyses have the potential to shed light upon changes in isotope composition of a magma during crystal growth, e.g., magma mixing and/or interaction with crustal lithologies. In this study, we present coupled major element and *in situ* Sr isotope data of plagioclase from a composite profile at the Union Section and Bellevue, covering the entire stratigraphy of the Bushveld Complex with the aim of constraining key petrogenetic aspects of the largest layered intrusion on Earth.

GEOLOGY OF THE BUSHVELD COMPLEX

Four main groups of igneous lithologies are recognised in the Bushveld Complex: (1) felsic volcanic rocks of the Rooiberg Group, (2) granites and granophyres of the Rashoop Granophyre Suite, (3) granitic rocks of the Lebowa Granite Suite and (4) layered mafic-ultramafic rocks of the Rustenburg Layered Suite (RLS) as the most voluminous group (Eales & Cawthorn, 1996). The complex covers an area of approximately 450 km x 350 km, for a total areal extent of > 65,000 km² with a recorded stratigraphic thickness of up to 8 km in the eastern part of the Bushveld. The RLS crops out in four different areas, known as limbs, with a fifth under younger sedimentary cover. These include the far-western, western, northern, eastern and the covered southern limbs (Fig. 1).

The mafic-ultramafic rocks of the RLS were emplaced discordantly into Neoarchean to Paleoproterozoic sedimentary rocks of the Transvaal Supergroup and Archean basement granites and gneisses at 2,055.91 ± 0.26 Ma based on U-Pb dating of zircon from a quenched marginal rock by Zeh *et al.* (2015). In comparison, Scoates & Wall (2015) presented U-Pb age dates of zircon from the overlying Merensky Reef with 2,056.88 ± 0.41 Ma for the western limb and 2,057.04 ± 0.55 Ma for the eastern limb, respectively. A standard zonal subdivision into five distinct major units has been traditionally accepted for the RLS (Hall, 1932). The noritic Marginal Zone at the bottom, followed by the ultramafic Lower Zone, the mafic-ultramafic Critical Zone, the gabbronoritic Main Zone and the ferrogabbroic Upper Zone at the top. The exact stratigraphic position of several zone boundaries remains contentious (Kruger, 1990; Mitchell, 1990). Historically, the zonal subdivision of the Bushveld Complex was mainly based on obvious changes in mineralogy, and subsequent whole rock Sr isotopic studies have shown that changes in isotope compositions broadly correspond to the mineralogical changes. Kruger (1994) interpreted the Bushveld Complex to have formed during two principle stages: (1) the *Integration Stage,* represented by the lower part of the complex

(Lower Zone, Critical Zone and the lower part of the Main Zone), was characterised by open-system conditions with multiple isotopically distinct influxes of magma and (2) the *Differentiation Stage,* which proceeded mainly under closed-system conditions, was dominated by large-scale fractional crystallisation and limited additions of new magma (upper part of the Main Zone and Upper Zone). For obvious reasons, we subsequently use major shifts in Sr isotopes for the definition of zone boundaries, as initially proposed by Kruger (1990).

Evidence for the addition of geochemically distinct pulses of magma led to several detailed studies on the parental magma composition of the Bushveld Complex. The main focus of these studies have been quenched marginal rocks and related fine-grained sills exposed in the floor of the intrusion (Davies *et al.*, 1980; Cawthorn *et al.*, 1981; Sharpe, 1981; Harmer & Sharpe, 1985; Barnes *et al.*, 2010). However, more recently, drill cores intersecting the lower contact of the igneous succession demonstrated the presence of relatively fresh chilled margins (Wilson, 2012; Maier *et al.*, 2016).

Sharpe (1981) established the widely accepted classification of Bushveld parental magmas in three suites: (i) Bushveld 1 (B1) magma underlying the Lower Zone, (ii) B2 magma underlying the Upper Critical Zone and (iii) B3 magma underlying the Main Zone. Recent studies by Wilson (2012) and Maier *et al.* (2016) suggested that the B1 magma represented a komatiitic magma with 18 - 19 wt % MgO, derived from the asthenosphere, which has been contaminated by crustal lithologies underlying the Bushveld Complex, whereas the B2 and B3 magmas were interpreted to represent tholeiitic basalts with $\sim$ 8 wt % MgO (Sharpe, 1985).

The floor rocks of the Bushveld Complex are mainly composed of Archean basement as well as chemical and siliciclastic sedimentary rocks of the Transvaal Supergroup, which were deposited from ca. 2,642 to 2,056 Ma (Scoates & Wall, 2015; Walraven & Martini, 1995). The lower part of the Transvaal Supergroup is known as the Chuniespoort Group and consists

of an approximately 2-km-thick succession of carbonate rocks at the base, comprising the Malmani Subgroup, which gives way to the Penge Iron Formation further up in the sequence (Eriksson et al., 2006). The upper part of the Transvaal Supergroup marks the transition from predominantly chemical sedimentation in the Chuniespoort Group to siliciclastic sedimentation in the 6 to 7-km-thick Pretoria Group. The latter mainly consists of shale alternating with quartzite, basaltic-andesitic lava, minor conglomerate, diamictites and carbonate rocks (Button, 1973; Eriksson *et al.,* 2006). Even though the western and eastern limbs of the Bushveld Complex were emplaced into siliciclastic Pretoria Group lithologies, providing no direct evidence for the interaction between Bushveld parental magmas and the underlying Chuniespoort Group, the magmas must have passed through the laterally extensive Malmani carbonate platform before final emplacement (Beukes, 1987; Eriksson *et al.*, 2006). In fact, the northern limb cuts across the Transvaal Supergroup from south to north. The floor rocks in the southern portion of the limb consist of Pretoria Group siliciclastic lithologies, whereas the central portion is dominated by dolomitic lithologies of the Chuniespoort Group, which give way to the underlying Archean basement granites and gneisses further north (Buchanan *et al.,* 1981).

SAMPLES AND ANALYTICAL METHODS

The thirty-seven samples used for this study are from the western and northern limbs of the Bushveld Complex. The Marginal, Lower and Critical zones were sampled from drill cores NG1, NG2 and NG3, respectively, whereas the Main Zone samples were taken from the exploration drill core SK-2. All these boreholes were drilled at the Union Section of the western Bushveld Complex (Fig. 1). The Upper Zone samples are from the Bellevue drill core BV-1, drilled in the northern limb of the intrusion. The Union Section samples were previously described in detail by Teigler (1990) and Mitchell (1990), whereas Barnes *et al*. (2004) and

Ashwal *et al.* (2005) provided petrographic descriptions and geochemical data for the Upper Zone samples from the Bellevue core.

A major reversal in mineral compositions coupled with a shift in Sr isotopic signature at the level of the Pyroxenite Marker is taken to represent the boundary between the Main Zone and the Upper Zone. This transition can be clearly pinpointed in the eastern and western limbs, whereas in the northern limb the boundary has not been defined so far. Ashwal *et al.* (2005) described two pyroxene-rich layers and a thick troctolitic horizon in the BV-1 drill core. However, the authors argued that neither of these represent the equivalent of the Pyroxenite Marker from the eastern or western limbs. A common stratigraphic feature among all three limbs is the first appearance of cumulus magnetite in the Upper Zone, which we use in the present study to correlate both drill sections (cf. Ashwal *et al.*, 2005). This marker horizon occurs some 550 m above the Pyroxenite Marker at the Union Section, whereas in drill core BV-1 from the northern limb this level corresponds to a depth of 1575.8 m (Ashwal *et al.*, 2005; Mitchell, 1990). The uppermost Main Zone sample was collected 250 m below the Pyroxenite Marker at the Union Section. To ensure sample coverage between the uppermost Main Zone sample and the first appearance of cumulus magnetite, the lowermost sample from the northern limb was collected about 400 m below the first appearance of cumulus magnetite. Therefore, the entire profile of the Bushveld Complex should be represented in the studied sample set, covering some 6.4 km of igneous stratigraphy.

The analysis of *in situ* Sr isotope compositions of plagioclase was conducted on a Photo Machine Analyte G2 laser microprobe coupled to a Nu Plasma HR multicollector inductively coupled mass spectrometer (LA-MC-ICP-MS) at the Geological Survey of Finland in Espoo. The analytical conditions were largely similar to those reported by Yang *et al.* (2013), who used a slightly modified methodology from that described by Ramos *et al.* (2004, 2005). The analyses were produced in static ablation mode using a beam diameter of 145 to 200 µm, a

pulse frequency of 10 Hz and a beam intensity of 2.07 J/cm^2. The samples were ablated in a HelEx ablation cell with a He gas flow of 0.4 and 0.1 l/min. The multicollector ICP-MS is fitted with 9 Faraday detectors and amplifiers with $10^{11}\Omega$ resistors and it was set up to measure the following isotopes ^{84}Sr-Kr, ^{85}Rb, ^{86}Sr-Kr, ^{87}Rb-Sr and ^{88}Sr in static mode. Correction of the instrument fractionation was performed using an exponential law and a ^{86}Sr/^{88}Sr ratio of 0.1194. Moreover, the isobaric interference of ^{87}Rb on ^{87}Sr was corrected with the ^{85}Rb signal and a ^{87}Rb/^{85}Rb ratio of 0.38571. Prior to each ablation, a background measurement of 30 s allowed for the correction of the isobaric interference of ^{86}Kr on ^{86}Sr. The measured isotope ratios were then age-corrected to 2,055 Ma using the ^{87}Rb/^{86}Sr ratio and a ^{87}Rb decay constant of 1.393 x 10^{-11} y^{-1} (Nebel *et al.*, 2011).

The average total Sr signal obtained for plagioclase samples was 0.4 V. Under these conditions, 120 s of ablation were needed to obtain an internal precision of $\leq \pm$ 0.000070 (1σ). The repeated analysis of an in-house plagioclase standard after approximately every ten measurements on the sample verified the accuracy of the LA-MC-ICP-MS protocol (Fig. 2). The in-house plagioclase standard (MIR a) is an isotopically homogeneous plagioclase megacryst from a lava of the Dutsin Miringa Hill volcano (Northern Cameroon Line) and has a reference ^{87}Sr/^{86}Sr ratio of 0.703096 $\pm$ 0.000070 (2σ, Rankenburg *et al.*, 2004) determined by conventional thermal ionisation mass spectrometry (TIMS). The measurement of the standard throughout the entire analytical session yielded an average ^{87}Sr/^{86}Sr ratio of 0.703106 $\pm$ 0.000090 (2σ, n = 85), which is in accordance with the reference ratio of the standard. Multiple analyses of the USGS Microanalytical Reference Material BHVO-2G (^{87}Rb/^{86}Sr = 0.065) gave an average ^{87}Sr/^{86}Sr ratio of 0.703476 $\pm$ 0.000139 (2σ, n = 10), which agrees with the GeoREM preferred value of 0.703469 $\pm$ 0.000014 (2σ, Elburg *et al.*, 2005). Since the Rb/Sr ratio of the reference material BHVO-2G is an order of magnitude higher than that of the ana-

lysed plagioclase crystals and the in-house plagioclase standard (MIR a), the Rb interference correction within the Rb/Sr range of the samples is validated.

Major element compositions of plagioclase were determined, using a Zeiss Sigma HD Analytical Field Emission Gun SEM equipped with two Oxford Instruments 150 mm^2 EDS detectors at Cardiff University. Analyses were carried out, using an accelerating voltage of 20 kV, 2.5 nA beam current, a spot size of 10 μm and a counting time of 30 s. Natural minerals and synthetic metals from Astimex Ltd. were used for calibration. Plagioclase from the same supplier was measured during the analytical runs to monitor instrumental drift.

The distribution of the ablation pits on each sample was intended to cover cumulus and intercumulus plagioclase grains as well as to record core-rim variations across individual grains. The corresponding major element compositions of the plagioclase grains were mostly obtained from the ablation pits themselves, and subsequently compared to analyses of areas surrounding the ablation pit in order to check the validity of the pit analysis.

RESULTS

While the *in situ* analyses of Sr isotopes in plagioclase broadly reproduces the whole rock Sr isotopic variation across all zones of the Bushveld Complex, certain differences were also revealed. The weighted average *in situ* Sr isotopic variation, together with the corresponding anorthite contents and its FeO concentrations, are shown in Figure 3 and Table 1. Additionally, Figure 4 shows the individual *in situ* analyses coupled with anorthite contents for every sample. The full dataset of the analyses is provided in the electronic appendix.

Lower Zone

The analysed samples from the ultramafic Lower Zone (LZ) mainly comprise dunite, harzburgite, pyroxenite, norite and gabbronorite. Generally, norites are rather unusual in the LZ and their origin remains elusive. According to Teigler (1990), norite occurs as a thin interval

of 2.9 m in thickness hosted by typical LZ pyroxenite. The initial *in situ* $^{87}Sr/^{86}Sr$ ratio of pla-gioclase at 2,055 Ma (Sr_i) in the LZ covers a relatively wide range from 0.7037 to 0.7077 (Fig. 4 a). Variations in anorthite content are even more pronounced, ranging from 38.2 to 79.0 mol %, excluding the norite sample, which contains cumulus plagioclase (NG2-300). This sample has a weighted average *in situ* Sr_i ratio of 0.7056 ± 0.0002 and an anorthite con-tent of 83.8 ± 0.9 mol %. The weighted average *in situ* Sr_i ratios show a relatively small, yet gradual upward increase from 0.7044 at the base to 0.7056 at 474 m (Fig. 5). The next two samples, analysed at 593 and 639 m, have a much higher average Sr isotope composition, reaching 0.7073 and 0.7071, respectively. Notably, this excursion in Sr_i ratios does not corre-late with any variation in trace element ratios or Mg# (100 x molar Mg/(Mg+Fe)), even though the anorthite content of these two samples are in line with the general upward increase (Figs. 5, 6).

Critical Zone

All the analysed samples from the Lower Critical Zone (LCZ) are pyroxenites with interstitial plagioclase, showing *in situ* Sr_i ratios from 0.7040 to 0.7061 (Fig. 4 b). The An content of the analysed grains show considerable variation, ranging from 48.8 to 73.6 mol %. The weighted average *in situ* Sr_i ratios cover a relatively narrow range, varying from 0.7049 to 0.7055, showing little change with stratigraphic height (Fig. 7).

The transition from the Lower to the Upper Critical Zone (UCZ) is defined by the first appearance of cumulus plagioclase. The analysed UCZ samples comprise two anorthosites, a norite and a pyroxenite with variable amounts of chromite. The *in situ* Sr isotope composition of cumulus plagioclase ranges from 0.7051 to 0.7066 (Fig. 4 b), whereas anorthite contents vary from 74.0 to 82.8 mol %. The weighted average *in situ* Sr_i ratios exhibit a more limited variation, ranging from 0.7058 to 0.7062. They show a sharp upward increase and no clear correlation with the anorthite contents or trace element ratios (Figs. 7, 8). The Sr_i ratio of in-

tercumulus plagioclase from the pyroxenite ranges from 0.7056 to 0.7067 with an average of 0.7061 ± 0.0003, which is similar to the Sr isotopic signature of cumulus plagioclase from this zone. The anorthite content is generally lower with 74.7 ± 1.5 mol %.

Main Zone

The principle rock types in the Main Zone (MZ) are layered olivine-free (leuco)-gabbronorite and minor norite, containing at least 50 vol % subhedral to euhedral plagioclase laths of up to 5 mm in length. The lowermost sample from this zone (A297) is a pyroxenite with < 5 vol % interstitial plagioclase. Sample A238 has a much larger grain size compared to the other ana-lysed MZ samples. Petrographically, it is a gabbronorite, but the plagioclase grains are mostly anhedral to subhedral, showing strong zonation. The *in situ* Sr isotope composition of all samples from the MZ, except for sample A238, ranges from 0.7081 to 0.7097, whereas the anorthite content varies from 56.8 to 71.5 mol % (Figs. 4 c, 9). In contrast, sample A238 shows considerably lower Sr_i ratios of 0.7071 to 0.7082 with anorthite contents from 54.5 to 65.9 mol %. The weighted average *in situ* Sr_i ratios within the MZ broadly decrease upwards, showing a positive correlation between anorthite content, trace element ratios and *in situ* Sr isotopes, except for sample A238 (Fig. 8). The lowermost sample from the MZ (A297) has a slightly lower anorthite content due to intercumulus plagioclase in the pyroxenite.

Upper Zone

The analysed Upper Zone (UZ) samples are represented by (magnetite-)gabbroic rocks with minor magnetitite. The variation of the *in situ* Sr isotope composition of plagioclase is rela-tively small, ranging from 0.7067 to 0.7084 (Fig. 4 d). The average anorthite contents cover a range from 46.4 to 66.0 mol %, showing a general upward decrease, whereas the weighted average *in situ* Sr isotope composition of plagioclase varies only slightly from 0.7073 to 0.7076 (Fig. 10). There is no clearly distinguishable stratigraphic trend in the *in situ* Sr iso-

topes across the UZ as all Sr_i ratios fall within error of the mean value of ~ 0.7074. Whole rock Sr isotope data for UZ samples from the western limb, analysed by Kruger *et al.* (1987), are only marginally lower with ~ 0.7073.

Summary

Distinct changes in Sr_i ratios are evident across the different zones of the Bushveld Complex (Fig. 3). Intercumulus plagioclase from the LZ is characterised by relatively constant Sr_i ratios and FeO concentrations in plagioclase, except for the uppermost sample of the LZ. The anorthite contents show no clear stratigraphic trend, resulting in a lack of correlation between Sr_i ratios and anorthite content or trace element ratios (Figs. 5, 6, 8). In the LCZ, the Sr_i ratio shows a reversal to ratios typical for the lower part of the LZ and then shows a slight upward increase. The FeO concentrations in plagioclase exhibit a gradual increase towards the top of the LCZ. Variation in anorthite contents is rather limited, although they seem to correlate with Sr_i ratios (Fig. 6). A sharp decrease in FeO concentrations in plagioclase occurs at the base of the UCZ, which correlates with a reversal towards lower anorthite contents. However, anorthite contents are generally much higher than in the LCZ. The Sr_i ratios increase slightly from the base to the middle of the zone before they increase significantly at the top of the UCZ. Accordingly, a correlation between Sr_i ratios and anorthite content is not evident (Fig. 11). The lower part of the MZ has the highest Sr_i ratios of the complex, whereas the overlying rocks show a progressive upward decrease in Sr_i ratios. The FeO concentrations in plagioclase remain relatively constant across the MZ, whereas the anorthite contents increase slightly from the base upwards before they gradually decrease in the upper part of the MZ, resulting in a broad correlation between anorthite contents and Sr_i ratios (Figs. 9, 12). An exception is sample A238 from the lower part of the MZ, which has much lower Sr_i and anorthite contents than the other MZ samples, even though the FeO concentrations in plagioclase are within the range of the other MZ samples. The Upper Zone is characterised by lower Sr_i ratios compared

to the MZ, exhibiting a sharp increase in anorthite contents and FeO concentrations in plagioclase, both of which gradually decrease towards the top of the zone. Ce/Sm has proven to be a useful trace element ratio in the discrimination of Bushveld lithologies (e.g., Maier *et al.*, 2013). It is worth noting that the Ce/Sm$_N$ ratios across the LZ and CZ are mostly above 2, whereas the MZ is characterised by Ce/Sm$_N$ ratios below 2 (Fig. 3). Even though the MZ has the least fractionated Ce/Sm$_N$ ratios, it features the highest Sr$_i$ ratios. The UZ shows the highest variation in Ce/Sm$_N$, ranging from 1 to 4.

DISCUSSION

Sr isotope disequilibrium between coexisting minerals

The *in situ* Sr isotope composition of plagioclase frequently shows more radiogenic Sr signatures than the respective whole rock analysis. This becomes especially apparent in the MZ as the gabbronorites contain high amounts of plagioclase in contrast to ultramafic rocks from the LZ or CZ, which have only limited amounts of plagioclase (< 10 vol %). Several studies attributed this to disequilibrium between coexisting minerals, where pyroxene would have a different Sr isotope composition than plagioclase in the same sample (Eales *et al.*, 1990a; Roelofse & Ashwal, 2012; Seabrook *et al.*, 2005; Yang *et al.*, 2013). Only Chutas *et al.* (2012) reported *in situ* Sr isotope data of both plagioclase and orthopyroxene, confirming the existence of disequilibrium. Another possible reason for the difference between whole rock and *in situ* Sr isotope data could be the excessive effect of age-correction on whole rock samples, containing K-rich minerals with relatively high Rb/Sr ratios like alkali feldspar, amphibole and mica, as the Rb/Sr ratio is directly included in the correction.

A mass balance calculation for a typical MZ gabbronorite (sample A1), using its mineral mode from Mitchell (1986), the *in situ* Sr isotope composition of plagioclase and Sr concentrations in the respective mineral shows that the Sr$_i$ ratio of pyroxene would have to be

unrealistically low (Sr_i = ~ 0.6969) in order to reproduce the whole rock Sr isotope composition (Table 2). Accordingly, a model envisaging Sr isotope disequilibrium between plagioclase and coexisting pyroxene based on whole rock Sr analyses appears rather implausible because of the extremely small Sr contribution from pyroxene to the whole rock Sr budget (~ 350 ppm Sr in plagioclase vs. < 30 ppm Sr in pyroxene). Regarding the presence of minerals with high Rb/Sr ratios, Roelofse (2010) reported ~ 4 vol % biotite and up to 12 vol % amphibole associated with pyroxene alteration in samples from the MZ. Furthermore, De Klerk (1982, 1991) and Teigler (1990) provided mineralogical modes of CZ and LZ samples, indicating similar modal abundances of mica.

On the basis of mass balance calculations and the consistent gap between *in situ* and whole rock Sr analyses in the MZ, we suggest that the gap partly results from an excessive age-correction of the whole rock data due to the presence of variable amounts of secondary mica and amphibole in the samples. We envisage that the alteration occurred in response to the introduction of small amounts of fluid along cracks, fissures and grain boundaries, which had an effect on the mineralogy, resulting in the formation of minerals with high Rb/Sr ratios as well as Rb concentrations, which significantly increase the amount of ^{87}Sr being subtracted during age-correction of the whole rock sample as shown in Table 2. In addition, these secondary minerals may also have a different isotope composition, reflecting that of the fluid. In contrast to whole rock analyses, these altered areas can be largely avoided with *in situ* analyses by focusing on clean and pristine areas of each analysed grain. Thus, the effect of this heavily depends on the modal mineralogy of the analysed sample: high amounts of plagioclase will result in a larger offset compared to samples with little plagioclase.

Intra-sample Sr isotope variations

Figure 13 shows the standard deviation of the *in situ* Sr_i ratios across the analysed profile of the Bushveld Complex. They are highly variable and largely independent of plagioclase tex-

tures, i.e., cumulus (UCZ, MZ, UZ) vs. intercumulus (LZ, LCZ) plagioclase. A correlation between specific zones and systematically more pronounced intra-sample variations is not evident from the dataset. Elevated standard deviations in certain zones would suggest that more than one isotopically distinct plagioclase population is present in a sample. However, the highly erratic behaviour of the standard deviations, even within a single zone, indicates that this is not the case.

Our data show compositional variations between cores and rims of individual plagioclase grains, but these compositional trends are rather erratic and many grains show somewhat ambiguous primary core-rim variations. Due to the absence of clear visual plagioclase zonation, it is difficult to determine whether the rim was actually formed after the core, especially in samples with interstitial plagioclase. Back-scatter electron imaging does not always allow for an unambiguous determination of growth zones, whereas high-resolution EDS-based elemental mapping reveals complex zonation patterns in cumulus and intercumulus plagioclase.

Formation of the Lower Zone

Teigler (1990) reported plagioclase and orthopyroxene compositions as well as bulk geochemistry for the LZ. The anorthite contents are highly erratic throughout the LZ, showing no distinct trend (Fig. 5). In contrast, the Mg# of orthopyroxene shows more subdued variation, except for the basal 50 m of the LZ, where the Mg# varies from 80.9 to 86.1. Between 50 to 210 m, the Mg# gradually decreases from 88.5 to 84.8, followed by a sharp increase to 89.4 at 265 m. Subsequently, the Mg# in orthopyroxene gradually decreases with a number of minor reversals. The bulk Mg# shows relatively little variation across the LZ, though there are fewer data in comparison to Mg# in orthopyroxene. The Sr_i ratios show relatively large variations over narrow stratigraphic intervals (Fig. 5). Nevertheless, a general upward increase in Sr_i ratios is evident and a sharp rise in the uppermost two LZ samples. The more radiogenic signature of these samples could potentially be attributed to a local disturbance of the Sr isotope

composition of plagioclase by external fluids. However, whole rock Nd isotope data of the radiogenic interval (Maier *et al.*, 2000) also show a deviation towards slightly more enriched compositions (i.e. lower εNd) from the typical LZ and LCZ εNd value of -5.3 (Fig. 3). Due to the more limited mobility of Sm relative to Rb, it is rather unlikely that an external fluid was capable of changing not only the Sr isotope composition, but also the Nd isotope composition of the magma. Instead, the *in situ* assimilation of either host rock lithologies or the intrusion of more radiogenic magma, as proposed by Kruger (1994), could account for the deflection in Sr_i ratios. The *in situ* assimilation of relatively evolved host rocks (e.g., felsic volcanic rocks of the Rooiberg Group) would have strongly affected the trace element signature of the radiogenic samples, but trace element data from Maier *et al.* (2013) indicate that the LZ has a fairly homogeneous trace element signature (Fig. 5). Figure 8 shows no correlation between Ce/Sm and Sr_i ratios, thus confirming that bulk contamination is unlikely to account for the shift in Sr_i ratios in the upper part of the LZ. In contrast, the influx of a more radiogenic mafic magma would not necessarily have a significant effect on the trace elements, although the Sr isotope composition would be affected. This model is consistent with the fact that the trace element signature and mineral compositions of the LZ lithologies show no geochemical difference between less and more radiogenic pyroxenites. Eales *et al.* (1990b) argued on the basis of Sr isotopes and reversals in mineral compositions that the LZ and CZ were subjected to repeated incursions of primitive mafic magma. Our results are largely in agreement with this model; however, based on our *in situ* Sr isotope work coupled with detailed elemental maps of interstitial plagioclase, we propose a two-stage formation for the LZ cumulates.

We envisage the formation of a proto-cumulate, predominantly consisting of mafic minerals, i.e. olivine and/or orthopyroxene, that was either emplaced in a series of crystal mushes or possibly crystallised *in situ* from repeated incursions of primitive magma. After the formation of the mafic framework, interstitial plagioclase crystallisation commenced, reflect-

ing the Sr isotope composition of the magma from which it crystallised. However, the large variations in Sr isotope compositions and the distinct zonation patterns of interstitial plagioclase (Fig. 14 a, b) strongly argue against undisturbed crystallisation of plagioclase from a trapped interstitial liquid. The complex zonation patterns suggest multiple influxes of melt into the mafic framework, mixing with and displacing some of the resident interstitial melt. Each of these influxes produced an isotopically distinct rim around earlier plagioclase crystals (Karykowski & Maier, 2017). Therefore, some interstitial plagioclase did not crystallise from the same melt that produced the mafic framework, explaining the large intra-sample variation in Sr isotope compositions. The weighted average Sr isotope composition provides an insight into the proportions of less radiogenic to more radiogenic magma involved in the formation of interstitial plagioclase.

The relatively primitive, yet radiogenic signature of the magma, from which the interstitial plagioclase crystallised, may have been acquired from the assimilation of the underlying Malmani dolomite in a staging magma chamber. Swart (1999) reported highly variable Sr concentrations for carbonate rocks from the Transvaal Supergroup, ranging from 10 to 629 ppm at relatively low REE concentrations (La < 10 ppm). Despite limited available Sr isotope data from the Malmani dolomite, data from Swart (1999) indicate that Transvaal Supergroup dolomite has a relatively radiogenic Sr isotope composition of 0.719 ± 0.012 (n = 7). These values are generally in agreement with Malmani data from Veizer *et al.* (1992) who reported Sr isotope compositions of 0.717 ± 0.005 (n = 10). The contamination of a B1-type parental magma with 175 ppm Sr and $Sr_i = 0.703$ (Harmer and Sharpe, 1985) by dolomite with 200 ppm Sr and $Sr_i = 0.718$ (average Sr concentration of Transvaal Supergroup carbonate rocks in the Transvaal Basin, as reported by Swart, 1999) shows that relatively high degrees of contamination (~ 37 %) are required to produce the most radiogenic Bushveld cumulates (Sample A271 from the Main Zone with $Sr_i = 0.7091$). For the most radiogenic LZ sample, the de-

gree of contamination would still be as high as 26 %. Such degree of contamination appears rather unrealistic and it would have probably affected the trace element signature, which is not observed. Alternatively, the addition of a CO_2- and Sr-rich fluid released during the decarbonation of dolomite, as proposed by Ganino *et al.* (2008, 2013b), may have also produced the geochemical characteristics of the staging magma without the necessity of bulk assimilation or partial melting.

According to Phinney (1992), the two main factors influencing the FeO concentrations in plagioclase are (1) oxygen fugacity and (2) polymerisation of the magma (Lundgaard & Tegner, 2004). Hence, it seems plausible that the magma, responsible for the excursion in Sr isotopes, was characterised by a higher oxygen fugacity. Ganino *et al.* (2008) showed that the interaction between a mafic magma and a fluid derived from the decarbonation of a sedimentary floor rock caused a significant increase in oxygen fugacity. Therefore, it is conceivable that the melt, percolating through parts of the mafic LZ framework, may have interacted with a fluid derived from the Malmani dolomite, which resulted in a high oxygen fugacity and possibly an elevated Sr isotope composition of the magma. This model remains difficult to verify as fluid compositions are not very well constrained to date, but Pronost *et al.* (2008) reported unradiogenic Sr isotope compositions of ≈ 0.704 for thermally-overprinted Malmani dolomite sample. However, the fluid may potentially be somewhat similar in composition to slab-derived fluids related to subduction zones, which are enriched in elements considered to be mobile (LILE, Ba, Pb, Sr) during slab-wedge transfer (e.g., Hoogewerff *et al.*, 1997). Notably, many back-arc basalts have a distinct slab signature, such as relatively radiogenic Sr isotope compositions and elevated incompatible element concentrations in comparison to magmatic rocks associated with mantle melting (e.g., Hawkesworth *et al.*, 1993; Spandler & Pirard, 2013). Regardless of the exact mechanism, varying volumes of more radiogenic melt,

percolating through the mafic LZ framework, controlled the Sr isotope composition of interstitial plagioclase.

Formation of the Lower Critical Zone

Teigler's (1990) mineral composition and whole rock data for the LCZ show an erratic, but gradual increase in anorthite contents from the base upwards (Fig. 7). Conversely, the Mg# of orthopyroxene remains constant from the base of the LCZ to 1,140 m, but the Mg# gradually decreases across the upper part of the LCZ. The bulk Mg# shows a similar trend compared to the Mg# of orthopyroxene. As the LCZ has a relatively unradiogenic Sr isotope composition compared to the uppermost portion of the LZ, interstitial plagioclase in the LCZ mostly formed from less radiogenic magma. However, the intra-sample range in Sr isotope compositions indicates that multiple isotopically distinct influxes of melt percolated through the mafic framework of the LCZ (Fig. 14 a, b). In fact, the intra-sample variation in Sr isotope compositions suggests a two end-member magma mixing trend between two relatively unradiogenic magmas across the LCZ, ranging from 0.705 to 0.706. In addition, the central part of the LCZ (samples NG1-327 and NG1-575) shows evidence for another later episode of melt percolation by even less radiogenic, yet relatively evolved magma with $Sr_i \sim 0.704$.

Implications for the formation of the Upper Critical Zone

All the UCZ samples from this study have a very narrow range in average *in situ* Sr_i ratios. The Sr_i ratios and An contents of cumulus plagioclase broadly overlap with those of Yang *et al.* (2013) from the footwall of the UG1 chromitite (Fig. 11). The overlying UG1 and Merensky footwall samples have slightly higher average Sr_i ratios, which increase even further through the Merensky Cyclic Unit (MCU) to the Bastard Cyclic Unit (BCU). The uppermost sample from the BCU, the Bastard anorthosite, has a similar average Sr_i ratio to plagioclase separates from the MZ analysed by Seabrook *et al.* (2005) and Roelofse (2010), respectively.

When considering Sr_i ratio ranges, representing all *in situ* Sr analyses of a particular zone, it is worth noting that these ranges shift from lower to higher Sr_i ratios with height, e.g. the MCU range is considerably lower than the BCU range, which shows some overlap with the lower-most two MZ samples from this study. Regarding the formation of the UCZ, Barnes & Maier (2002) as well as Wilson & Chunnett (2006) argued on the basis of trace element patterns that the MCU and BCU crystallised from a mixture between CZ and MZ magmas. In contrast, Seabrook *et al.* (2005) and Yang *et al.* (2013) suggested that these units were formed by the co-accumulation of plagioclase from two isotopically distinct reservoirs, i.e. CZ and MZ parental magmas.

In the case of the latter model, the result would be a binary distribution of Sr_i ratios, where modal abundances of plagioclase from each reservoir are the main factor, controlling the average Sr_i ratio of the sample. Hence, we would expect to see similar *in situ* Sr_i ranges in the MCU and BCU with varying average Sr_i ratios, depending on the modal abundances of plagioclase from each parental magma. Moreover, samples containing plagioclase from two distinct reservoirs would have much larger Sr_i standard deviations compared to samples containing plagioclase from a single source. The UCZ data from this study together with data from Yang *et al.* (2013) show that there is no systematic difference in standard deviations (2σ) between the lower part of the UCZ and the upper part, which has been proposed to contain two isotopically distinct plagioclase populations (Fig. 13). A broad overall decrease in standard deviations is evident across the analysed profile, which may reflect the upward increase of Sr concentrations in plagioclase, resulting in greater analytical precision (e.g., Cawthorn, 2007).

Our data suggest that the *in situ* Sr isotope composition of plagioclase from the MCU and BCU resulted from the crystallisation of plagioclase from a mixed magma of alternating composition rather than from the co-accumulation of plagioclase from two distinct reservoirs.

The lower part of the UCZ shows little evidence for magma addition and mixing, although the average Sr_i ratios increase slightly from the LCZ to the bottom of the UCZ. The first significant increase in Sr_i ratio occurs at the level of the UG1 chromitite. All overlying samples have gradually increasing Sr_i ratios, which is consistent with progressively increasing proportions of more radiogenic magma to the CZ parental magma, as proposed by Barnes & Maier (2002) as well as Wilson & Chunnett (2006). The gradual increase in average Sr_i ratios further suggests relatively protracted mixing or a slow addition of magma. Compositional variations in single cumulus plagioclase crystals, however, show highly complex zonation patterns, which may indicate continual ingress of geochemically distinct magma that picked up previously formed plagioclase crystals (Fig. 14 c).

Petrogenesis of the Main and Upper Zones

The orthopyroxene composition and the bulk Mg#, determined by Mitchell (1986) for MZ samples from the same drill core, show a similar trend to the *in situ* Sr isotope compositions with a progressive upward and downward decrease in Mg#, starting at approximately 2,400 m (Fig. 9). Whole rock samples, located stratigraphically below the lowermost sample analysed in this study (sample A297), show a dramatic downward decrease in whole rock Sr_i ratios, whereas anorthite contents remain relatively high. Although these observations have not been confirmed by *in situ* analyses, Sr isotope data of plagioclase separates from the base of the MZ in the eastern limb analysed by Seabrook *et al.* (2005) largely confirm the low Sr_i ratios and relatively high anorthite contents (Fig. 12). Accordingly, these results suggest that the lower portion of the MZ was still affected by the above mentioned mixing between CZ and MZ magma. Hence, this part of the MZ represents the continuation of the UCZ mixing trend with a strong contribution from the MZ magma. Based on Sr isotopic evidence, the entire mixing zone extends from 1,850 to 2,450 m, covering some 600 m in stratigraphy.

The *in situ* Sr isotope data from this study show a broadly positive correlation between anorthite contents and Sr_i ratios in the remainder of the MZ, suggesting a binary mixing between a relatively primitive, yet highly radiogenic component and a more evolved and less radiogenic component (Fig. 12). The gradual upward decrease in Sr_i ratios above sample A271 can thus be explained by progressive mixing between these two components. The primitive, highly radiogenic end-member would be the parental magma to the MZ, whereas the less radiogenic counterpart could be either UZ or CZ magma. The combination of "primitive" and "highly radiogenic" magma is rather atypical for classic crustal contamination models, as magmas generally become more fractionated with contamination, which also affects the Sr isotopic signature. Trace element ratios strongly argue against extensive upper crustal contamination of the MZ parental magma as Ce/Sm ratios in the MZ are generally lower than in the CZ and LZ (cf. Figs. 5, 7, 8, 9). Alternatively, it could be argued that the magma was contaminated by mid- to lower crustal lithologies (e.g., Lewisian gneisses). Granulite-facies gneiss from the Lewisian (ca. 2.9 Ga) has low Ce/Sm_N ratios of < 2 (Weaver & Tarney, 1980), but the Sr isotope composition at 2,055 Ma would have been too unradiogenic to produce the MZ signature (Dickin, 1981). In contrast, amphibolite-facies gneiss from the same complex shows Sr isotope compositions in the range of the MZ lithologies; however, Ce/Sm_N ratios of > 3.5 are clearly too high to explain those of the MZ (Dickin, 1981; Weaver & Tarney, 1980).

Despite the lack of indicators for crustal contamination, the Sr isotope composition of the MZ parental magma is highly elevated. This observation may be consistent with the contamination of the magma with a fluid, derived from dolomite, which may have increased the Sr isotope composition of the magma, while leaving the trace element budget largely unaffected.

VanTongeren & Mathez (2013) showed that the parental magma to the UZ was compositionally similar to the tholeiitic B2-type sills described by Harmer & Sharpe (1985) and therefore also to the CZ magma. Sharpe (1985) suggested that the MZ was emplaced on top of the CZ cumulate pile, leading to an upward displacement of the fractionated resident magma, which subsequently crystallised the UZ. According to VanTongeren & Mathez (2013), however, the CZ and the UZ magmas have similar source compositions, but both zones crystallised from different batches of magma. The model could explain the upward decrease in Sr_i ratios by mixing, but Kruger *et al.* (1987) and Cawthorn *et al.* (1991) argued that mixing between the residual CZ magma (eventually forming the UZ) and the relatively primitive MZ magma would not have preserved the isotopic discontinuity at the level of the Pyroxenite Marker, which also defines the base of the UZ in this study (Fig. 3). Instead, these authors suggested that the UZ crystallised from a new batch of magma, emplaced close to the top of the MZ cumulates, which mixed with resident magma from the MZ. Maier & Barnes (1998) proposed that the MZ magma intruded as a highly viscous crystal mush into semi-consolidated UCZ and UZ cumulate. This model, however, does not account for the gradual upward decrease in Sr isotope composition, which requires magma mixing within the MZ.

In light of the evidence, we propose that progressive mixing between MZ magma and either overlying resident CZ magma or fresh UZ magma occurred already from the lower portion of the MZ to the Pyroxenite Marker. Regardless of the exact derivation of the added magma, the observed variation in Sr_i ratios across the MZ can be explained by an incremental addition of tholeiitic B2-type magma to the resident MZ magma. Consequently, early cumulus plagioclase grains, characterised by relatively radiogenic compositions, were overgrown by less radiogenic plagioclase as indicated by Figure 14 c. This interpretation is further supported by the distinct correlation between most of the MZ samples and the UZ samples in Figure 8. In order to preserve the isotopic discontinuity at the level of the Pyroxenite Marker,

we agree that the UZ is likely to be the product of a separate pulse of B2-type magma with little to no addition of MZ magma. Evidence for the injection of UZ magma on top of the MZ cumulate pile is provided by the undulating contact between the MZ anorthosite and the Pyroxenite Marker with typical flame-like protrusions of anorthosite into the overlying gabbroids, described in the eastern limb of the Bushveld Complex (Fig. 2, Maier *et al.*, 2001). In the sedimentological research community, these structures are unequivocally interpreted to result from density contrasts between unlithified layers, where the underlying less dense layer pushes up into the overlying denser layer (e.g., Anketell *et al.*, 1970). This inversion in density is also present in the observed lithologies associated with the flame structures. Thus, we interpret these structures as an indication that the UZ was emplaced on top of a semi-consolidated MZ cumulate.

Comparison between the western and northern limb Main Zones

In comparison to the MZ from the northern limb studied by Mangwegape *et al.* (2016), the samples from this study have considerably lower anorthite contents, whereas Sr isotopic signatures are comparable (Fig. 12). One explanation for the higher anorthite contents in the northern limb may be the contamination of the MZ magma by the underlying Malmani dolomite, as the assimilation of dolomite or a partial melt thereof would have considerably increased the CaO concentrations in the magma, producing plagioclase with elevated anorthite contents relative to less contaminated portions of the magma chamber. Wenzel *et al.* (2002) proposed that a low viscosity calcite melt could be easily extracted at relatively low temperatures from a dolomitic protolith, whereas much of the MgO remained in the restite as periclase. This is further supported by the Mg# of pyroxene from the MZ, which shows very little variation among the three limbs of the Bushveld, suggesting nearly similar MgO concentrations in the magma.

Ganino *et al*. (2013a) showed that a partial melt derived from a dolomitic protolith can be highly enriched in REE. Such a process would have also changed the trace element ratios of the MZ magma. Trace element data from Roelofse (2010), however, indicate that there is no apparent difference in trace element signatures between the northern and western limb MZ. Hence, it is considered unlikely that the assimilation of a partial dolomitic melt in the northern limb led to an increase in CaO and therefore anorthite contents. In contrast, the interaction between a CO_2-rich fluid, released from dolomite during decarbonation, would probably not have been capable of introducing high amounts of CaO into the melt without changing its Sr isotopic signature.

Another explanation could be that most of the northern limb MZ represents a thick mixing zone between MZ and UCZ magma, similar to the eastern and western limbs of the Bushveld, but on a much larger scale. Figure 12 clearly suggests mixing between a potential end-member MZ magma and typical UCZ magma compositions. Notably, the Bastard anorthosite sample from the UCZ of the western limb analysed by Yang *et al*. (2013) plots well within the northern limb MZ range, suggesting that many of the northern limb MZ samples have an UCZ affinity in terms of Sr isotopic signature as well as anorthite contents. Some northern limb samples have even higher Sr isotope compositions than the proposed MZ magma ($\sim$ 0.7091), but this could be explained by local contamination of the magma by the granitic footwall. The zone of mixing essentially comprises lithologies close to the UCZ-MZ boundary with Sr_i ratios, ranging from $\sim$ 0.7080 to $\sim$ 0.7090. In the western limb, this zone is approximately 300-m-thick, whereas in the northern limb this zone covers more than 1,000 m in stratigraphy.

In the northern limb, the upward decrease in Sr_i ratios begins at a much higher stratigraphic level compared to the western limb, i.e., probably just below the troctolite horizon (cf. Fig. 4, Mangwegape *et al*., 2016). This may be the result of the increased thickness of the

UCZ-MZ mixing zone. Mangwegape *et al.* (2016) suggested that the upper part of the MZ and the entire UZ formed primarily in response to normal fractionation, which implies constant Sr isotope compositions; however, Figure 12 clearly shows a mixing trend between MZ and UZ magma similar to the western limb, but with a larger influence of the UCZ magma on the initial MZ composition in the northern limb.

We propose that the upper part of the northern limb MZ was also affected by the progressive addition of UZ magma in order to produce the upward decrease in Sr_i ratios similar to the western limb. Based on Sr isotope compositions and anorthite contents, the lower part of the northern limb MZ was seemingly subjected to several voluminous injections of CZ magma into the resident MZ magma.

Implications for intrusion emplacement

The interaction between the large volumes of magma that produced the Bushveld Complex and the 2-km-thick carbonate platform of the Transvaal Supergroup could also be considered as a possible mechanism to create space in the crust since the devolatilisation and dissociation of chemical sediments is directly linked to volume loss, i.e. the thermal decomposition of dolomite results in lower molar volumes, larger surface areas and greater porosities (e.g., Olszak-Humienik & Jablonski 2015). Hence, the vertical inflation of the Bushveld Complex, or parts thereof, may have been accommodated by floor depression in response to volume loss, thus producing a lopolith (e.g., Cruden, 1998).

Regional isotopic variation in the UCZ of the Bushveld Complex

Several authors have reported contrasting Sr isotope compositions for MCU and BCU cumulates in different parts of the Bushveld Complex. The MCU at the Rustenburg and Union sections in the western limb (Eales *et al.*, 1986; Kruger & Marsh, 1982) as well as at Richmond and Atok in the eastern limb (Seabrook *et al.*, 2005; Lee & Butcher, 1990) have Sr isotope

compositions typical of the CZ (Sr_i = ~ 0.7064), whereas the MCU at Amandelbult (Kruger, 1992) in the western limb has a more MZ-like signature (Sr_i = ~ 0.7075). Similar discrepancies were also reported for the BCU (Lee & Butcher, 1990, Seabrook *et al*., 2005). The Sr isotope data presented in this study indicate that the UCZ crystallised from a magma with a Sr_i ratio of ~ 0.7061, if not lower. Our data further suggest that the lower part of the MZ was still affected by mixing between CZ and MZ. Therefore, the initial influx of MZ magma before mixing would have had a Sr_i ratio of ~ 0.7091, if not higher (MZ sample A271). Thus, the proposed Sr isotope composition of the MZ magma differs dramatically from previously assumed ratios (Eales *et al*., 1986; Kruger & Marsh, 1982; Lee & Butcher, 1990; Seabrook *et al*., 2005), except for Kruger & Mitchell (1985) who suggested a Sr_i ratio of 0.7090 for the MZ. Consequently, we interpret the regional differences in Sr_i ratios to represent varying degrees of mixing in different portions of this very large magma chamber. The fact that none of the marginal sills from the Bushveld Complex (Harmer & Sharpe, 1985) provide evidence for the existence of a radiogenic MZ parental magma may simply reflect that the MZ is not represented in the suite of marginal rocks.

Regionally non-uniform mixing of magmas and the crystallisation of minerals in presumably cotectic proportions essentially produced a semi-consolidated cumulate pile with different isotopic signatures along the same stratigraphic level (Fig. 15 a, b). As proposed by Maier *et al*. (2013), these proto-cumulates may have been episodically mobilised by major slumping events associated with magma chamber subsidence, resulting in density-sorted crystal slurries. As a consequence, regional variations in the Sr isotope composition related to different degrees of magma mixing, before slumping and sorting, were preserved in the layered UCZ units (Fig. 15 c).

On iron-rich ultramafic pegmatites

One of the analysed samples from the MZ (sample A238) is an unusually coarse-grained gabbronorite, reaching up to 10 mm in grain size with an average *in situ* Sr_i ratio of ~ 0.7077, which is much lower than the average *in situ* Sr_i ratios of all other samples from the MZ (Fig. 9). The chondrite-normalised rare earth element (REE) diagram in Figure 16 shows that this sample has a distinct REE pattern in comparison to typical MZ lithologies. Instead, the REE pattern is similar to that of iron-rich ultramafic pegmatites (IRUP) from the UCZ, described by Reid & Basson (2002). These authors also reported whole rock Sr isotope data for two samples, averaging at $Sr_i = \sim 0.7074$. In addition, Scoon & Mitchell (1994) analysed IRUPs from the MZ for whole rock Sr isotope compositions. Their data confirm the lower range in Sr_i ratios, averaging at ~ 0.7076 (n = 10). Based on the similarities in terms of REE patterns and Sr isotopes, we conclude that sample A238 belongs to the IRUP group. Notably, the sample also shows a considerable incursion in anorthite contents and Mg# (Fig. 9), which Scoon & Mitchell (1994) interpreted to result from a trapped liquid shift. This proposed reaction between trapped liquid and cumulus minerals, cannot account for the observed shift in Sr_i ratios between MZ cumulates and IRUP sample A238.

Based on our limited data on this single IRUP sample, it is impossible to present a conclusive petrogenetic model, but the coarse grain size, the evolved mineral chemistry, the pronounced zonation of plagioclase and the distinct shift in Sr_i ratios indicate that the IRUP did not form from the same magma that crystallised the MZ, even though the sample is characterised by variable *in situ* Sr_i ratios (Fig. 4 c).

SUMMARY AND CONCLUSION

1. Detailed variations in Sr_i ratios across the layered sequence of the Bushveld Complex reveal subtle, yet important differences between whole rock and *in situ* Sr iso-

tope data. The latter commonly show more radiogenic compositions compared to the whole rock analysis, especially in the Main Zone. Our data indicate that this is not due to isotope disequilibrium between the rock-forming minerals, but due to an excessive age-correction, owing to the presence of secondary minerals with distinct Sr isotope compositions and high Rb/Sr ratios like mica and amphibole. Hence, age-corrected whole rock Sr isotope data may not always record the true Sr isotope composition of the sample.

2. Complex zonation patterns in interstitial plagioclase from the Lower Zone, together with large variations in Sr isotope composition, suggest multiple incursions of primitive magma with varying Sr_i ratios into a mafic proto-cumulate. Each of these influxes produced an isotopically distinct rim around earlier plagioclase crystals. The initial Lower Zone magma likely had a relatively unradiogenic Sr isotope composition of < 0.7046. Pulses of more radiogenic magma may have acquired its isotopic signature from the interaction with the dolomitic floor rocks. Decoupling of anorthite contents from *in situ* Sr_i ratios as well as constant trace element ratios across the Lower Zone do not support bulk assimilation of crustal lithologies to explain the more radiogenic composition. However, a fluid phase, released from the decarbonation of the dolomites, may have changed the Sr isotopic signature of the magma without affecting trace element ratios.

3. The Lower Critical Zone is slightly more radiogenic with Sr_i ratios of ~ 0.7054 compared to the majority of the Lower Zone cumulates. The intra-sample range in Sr isotope compositions indicates that multiple isotopically distinct influxes of melt percolated through the mafic proto-cumulate, similar to the Lower Zone.

4. The Upper Critical Zone shows a progressive increase in Sr_i ratios from the bottom to the top. *In situ* analyses indicate that the zone crystallised from a Critical Zone

magma mixed with progressively increasing proportions of Main Zone magma. Regional Sr isotopic variations in the Merensky Cyclic Unit and the Bastard Cyclic Unit are interpreted to be the result of non-uniform mixing between the two end-members.

5. The lowermost part of the Main Zone represents the continuation of the Upper Critical Zone mixing trend, but the mixed magma at this level was already dominated by the Main Zone end-member. The highest Sr_i ratio in this zone is also likely to be the initial Sr isotope composition of the Main Zone magma before mixing ($Sr_i > 0.7091$). Trace element ratios suggest no crustal contamination. The progressive addition of a less radiogenic magma towards the top of the zone is evident in the gradual upward decrease in Sr_i ratios, e.g., Upper Zone magma. The enigma of a highly radiogenic Main Zone magma, which shows no evidence for crustal contamination, suggests an unusual mechanism of contamination. These observations can be explained by contamination of the Main Zone magma with a dolomite-derived fluid in a staging magma chamber, similar to the upper part of the Lower Zone.

6. The Upper Zone crystallised from a distinct pulse of magma with a Sr isotope composition of ~ 0.7074 emplaced at the level of the Pyroxenite Marker. Fractional crystallisation proceeded with relatively limited disturbance, showing little evidence for the addition of an isotopically distinct magma.

7. The interaction between devolatising sedimentary rocks and magma may also be an important petrogenetic process in other mafic-ultramafic intrusions – not only as a control on magma composition, but also regarding magma emplacement mechanisms as devolatilisation is directly linked to space creation due to volume loss.

REFERENCES

Anketell, J. M., Cegla, J. & Dzulynski, S. (1970). On the deformational structures in systems with reversed density gradients. *Rocznik Polskiego Towarzystwa Geologicznego* **40**, 3–29.

Ashwal, L. D., Webb, S. J. & Knoper, M. W. (2005). Magmatic stratigraphy in the Bushveld Northern Lobe: continuous geophysical and mineralogical data from the 2950 m Belle-vue drillcore. *South African Journal of Geology* **108**, 199–232.

Barnes, S.-J. & Maier, W. D. (2002). Platinum-group elements and microstructures of Normal Merensky Reef from Impala Platinum Mines, Bushveld Complex. *Journal of Petrology* **43**, 103–128.

Barnes, S.-J., Maier, W. D. & Ashwal, L. D. (2004). Platinum-group element distribution in the Main Zone and Upper Zone of the Bushveld Complex, South Africa. *Chemical Geology* **208**, 293–317.

Barnes, S.-J., Maier, W. D. & Curl, E. A. (2010). Composition of the marginal rocks and sills of the Rustenburg Layered Suite, Bushveld Complex, South Africa: implications for the formation of the platinum-group element deposits. *Economic Geology* **105**, 1491–1511.

Beukes, N. J. (1987). Facies relations, depositional environments and diagenesis in a major early Proterozoic stromatolitic carbonate platform to basinal sequence, Campbellrand Subgroup, Transvaal Supergroup, Southern Africa. *Sedimentary Geology* **54**, 1–46.

Buchanan, D. L., Nolan, J., Suddaby, P., Rouse, J. E., Viljoen, M. J. & Davenport, J. W. J. (1981). The genesis of sulfide mineralization in a portion of the Potgietersrus Limb of the Bushveld Complex. *Economic Geology* **76**, 568–579.

Button, A. (1973). A regional study of the stratigraphy and development of the Transvaal Basin in the Eastern and Northeastern Transvaal. PhD thesis, Johannesburg, South Africa, University of Witwatersrand.

Cawthorn, R. G. (2015). The Bushveld Complex, South Africa. In: Charlier, B., Namur, O., Latypov, R. & Tegner, C. (eds) *Layered Intrusions*. Springer, 517–587.

Cawthorn, R. G., Davies, G., Clubley-Armstrong, A. & McCarthy, T. S. (1981). Sills associated with the Bushveld Complex, South Africa: an estimate of the parental magma composition. *Lithos* **14**, 1–16.

Cawthorn, R. G., Meyer, P. S. & Kruger, F. J. (1991). Major addition of magma at the Pyroxenite Marker in the western Bushveld Complex, South Africa. *Journal of Petrology* **32**, 739–763.

Chadwick, J. P., Troll, V. R., Ginibre, C., Morgan, D., Gertisser, R., Waight, T. E. & Davidson, J. P. (2007). Carbonate assimilation at Merapi Volcano, Java, Indonesia: Insights from crystal isotope stratigraphy. *Journal of Petrology* **48**, 1793–1812.

Charlier, B. L. A., Bachmann, O., Davidson, J. P., Dungan, M. A. & Morgan, D. J. (2007). The upper crustal evolution of a large silicic magma body: evidence from crystal-scale Rb–Sr isotopic heterogeneities in the Fish Canyon magmatic system, Colorado. *Journal of Petrology* **48**, 1875–1894.

Charlier, B. L. A., Ginibre, C., Morgan, D., Nowell, G. M., Pearson, D. G., Davidson, J. P. & Ottley, C. J. (2006). Methods for the microsampling and high-precision analysis of strontium and rubidium isotopes at single crystal scale for petrological and geochronological applications. *Chemical Geology* **232**, 114–133.

Chutas, N. I., Bates, E., Prevec, S. A., Coleman, D. S. & Boudreau, A. E. (2012). Sr and Pb isotopic disequilibrium between coexisting plagioclase and orthopyroxene in the Bushveld Complex, South Africa: microdrilling and progressive leaching evidence for subliquidus contamination within a crystal mush. *Contributions to Mineralogy and Petrology* **163**, 653–668.

Cruden, A. R. (1998). On the emplacement of tabular granites. *Journal of the Geological Society* **155**, 853–862.

Davidson, J. P., Morgan, D. J., Charlier, B. L. A., Harlou, R. & Hora, J. M. (2007). Microsampling and Isotopic Analysis of Igneous Rocks: Implications for the Study of Magmatic Systems. *Annual Review of Earth and Planetary Sciences* **35**, 273–311.

Davidson, J. P., Tepley III, F. J. & Knesel, K. M. (1998). Crystal isotope stratigraphy; a method for constraining magma differentiation pathways. *Eos Trans. Am. Geophys. Union* **79**, 185–189.

Davies, G., Cawthorn, R. G., Barton, J. M. & Morton, M. (1980). Parental magma to the Bushveld Complex. *Nature* **287**, 33–35.

De Klerk, W. J. (1982). The geology, geochemistry and silicate mineralogy of the Upper Critical Zone of the North-western Bushveld Complex, at Rustenburg Platinum Mines, Union section. MSc thesis, Grahamstown, South Africa, Rhodes University.

De Klerk, W. J. (1991). Petrogenesis of the Upper Critical Zone in the western Bushveld Complex with emphasis on the UG1 Footwall and Bastard units. PhD thesis, Grahamstown, South Africa, Rhodes University.

Dickin, A. P. (1981). Isotope geochemistry of Tertiary igneous rocks from the Isle of Skye, N.W. Scotland. *Journal of Petrology* **22**, 155–189.

Eales, H. V. & Cawthorn, R. G. (1996). The Bushveld Complex. In: Cawthorn, R. G. (ed.) *Developments in Petrology*. Elsevier, 181–229.

Eales, H. V., De Klerk, W. J., Butcher, A. R. & Kruger, F. J. (1990a). The cyclic unit beneath the UG1 chromitite (UG1FW unit) at RPM union section platinum mine - Rosetta stone of the Bushveld Upper Critical Zone. *Mineralogical Magazine* **54**, 23–43.

Eales, H. V., De Klerk, W. J. & Teigler, B. (1990b). Evidence for magma mixing processes within the Critical and Lower Zones of the northwestern Bushveld Complex, South Africa. *Chemical Geology* **88**, 261–278.

Eales, H. V., Marsh, J. S., Mitchell, A. A., De Klerk, W. J., Kruger, F. J. & Field, M. (1986). Some geochemical constraints upon models for the crystallization of the Upper Critical Zone–Main Zone interval, northwestern Bushveld Complex. *Mineralogical Magazine* **50**, 567–582.

Elburg, M., Vroon, P., van der Wagt, B. & Tchalikian, A. (2005). Sr and Pb isotopic composition of five USGS glasses (BHVO-2G, BIR-1G, BCR-2G, TB-1G, NKT-1G). *Chemical Geology* **223**, 196–207.

Eriksson, P. G., Altermann, W. & Hartzer, F. J. (2006). The Transvaal Supergroup and its precursors. In: Johnson, M.R., Anhaeusser, C.R., Thomas, R.J. (eds.) *The Geology of South Africa*. Geological Society of South Africa/Council for Geoscience, Johannesburg/Pretoria, 237–260.

Faure, G. (1986). *Principles of isotope geochemistry*. New York: John Wiley, 464 p.

Gagnevin, D., Daly, J. S., Poli, G. & Morgan, D. (2005). Microchemical and Sr isotopic investigation of zoned K-feldspar megacrysts: insights into the petrogenesis of a granitic system and disequilibrium crystal growth. *Journal of Petrology* **46**, 1689–1724.

Ganino, C., Arndt, N. T., Chauvel, C., Jean, A. & Athurion, C. (2013a). Melting of carbonate wall rocks and formation of the heterogeneous aureole of the Panzhihua intrusion, China. *Geoscience Frontiers* **4**, 535–546.

Ganino, C., Arndt, N. T., Zhou, M.-F., Gaillard, F. & Chauvel, C. (2008). Interaction of magma with sedimentary wall rock and magnetite ore genesis in the Panzhihua mafic intrusion, SW China. *Mineralium Deposita* **43**, 677–694.

Ganino, C., Harris, C., Arndt, N. T., Prevec, S. A. & Howarth, G. H. (2013b). Assimilation of carbonate country rock by the parent magma of the Panzhihua Fe-Ti-V deposit (SW China): Evidence from stable isotopes. *Geoscience Frontiers* **4**, 547–554.

Gao, J.-F., Zhou, M.-F., Robinson, P. T., Wang, C. Y., Zhao, J.-H. & Malpas, J. (2015). Magma mixing recorded by Sr isotopes of plagioclase from dacites of the Quaternary Tengchong volcanic field, SE Tibetan Plateau. *Journal of Asian Earth Sciences* **98**, 1–17.

Ginibre, C. & Davidson, J. P. (2014). Sr isotope zoning in plagioclase from Parinacota Volcano (Northern Chile): Quantifying magma mixing and crustal contamination. *Journal of Petrology* **55**, 1203–1238.

Hall, A. L. (1932). The Bushveld Igneous Complex of the central Transvaal. *Memoirs of the Geological Survey of South Africa* **28**, 530.

Harmer, R. E., Auret, J. M. & Eglington, B. M. (1995). Lead isotope variations within the Bushveld Complex, Southern Africa: a reconnaissance study. *Journal of African Earth Sciences* **21**, 595–606.

Harmer, R. E. & Sharpe, M. R. (1985). Field relations and strontium isotope systematics of the marginal rocks of the eastern Bushveld Complex. *Economic Geology* **80**, 813–837.

Hawkesworth, C. J., Gallagher, K., Hergt, J. M. & McDermott, F. (1993). Mantle and slab contribution in arc magmas. *Annual Review of Earth and Planetary Sciences* **21**, 175–204.

Hoogewerff, J. A. *et al.* (1997). U-series, Sr-Nd-Pb isotope and trace-element systematics across an active island arc-continent collision zone: Implications for element transfer at the slab-wedge interface. *Geochimica et Cosmochimica Acta* **61**, 1057–1072.

Karykowski, B. T. & Maier, W. D. (2017). Microtextural characterisation of the Lower Zone in the western limb of the Bushveld Complex, South Africa: evidence for extensive melt migration within a sill complex. *Contributions to Mineralogy and Petrology* **172**, 60.

Kruger, F. J. (1990). The stratigraphy of the Bushveld Complex; a reappraisal and the relocation of the Main Zone boundaries. *South African Journal of Geology* **93**, 376–381.

Kruger, F. J. (1992). The origin of the Merensky cyclic unit: Sr-isotopic and mineralogical evidence for an alternative orthomagmatic model. *Australian Journal of Earth Sciences* **39**, 255–261.

Kruger, F. J. (1994). The Sr-isotopic stratigraphy of the western Bushveld Complex. *South African Journal of Geology* **97**, 393–398.

Kruger, F. J., Cawthorn, R. G. & Walsh, K. L. (1987). Strontium isotopic evidence against magma addition in the Upper Zone of the Bushveld Complex. *Earth and Planetary Science Letters* **84**, 51–58.

Kruger, F. J. & Marsh, J. S. (1982). Significance of ^{87}Sr/^{86}Sr ratios in the Merensky cyclic unit of the Bushveld Complex. *Nature* **298**, 53–55.

Kruger, F. J. & Mitchell, A. A. (1985). Discontinuities and variations of Sr-isotope systematics in the Main Zone of the Bushveld Complex, and their relevance to PGE mineralization. *Canadian Mineralogist* **23**, 306–306.

Lee, C. A. & Butcher, A. R. (1990). Cyclicity in the Sr isotope stratigraphy through the Merensky and Bastard Reef units, Atok section, eastern Bushveld Complex. *Economic Geology* **85**, 877–883.

Liu, P.-P., Zhou, M.-F., Wang, C. Y., Xing, C.-M. & Gao, J.-F. (2014). Open magma chamber processes in the formation of the Permian Baima mafic–ultramafic layered intrusion, SW China. *Lithos* **184–187**, 194–208.

Lundgaard, K. L. & Tegner, C. (2004). Partitioning of ferric and ferrous iron between plagioclase and silicate melt. *Contributions to Mineralogy and Petrology* **147**, 470–483.

Maier, W. D., Arndt, N. T. & Curl, E. A. (2000). Progressive crustal contamination of the Bushveld Complex: evidence from Nd isotopic analyses of the cumulate rocks. *Contributions to Mineralogy and Petrology* **140**, 316–327.

Maier, W. D. & Barnes, S.-J. (1998). Concentrations of rare earth elements in silicate rocks of the Lower, Critical and Main Zones of the Bushveld Complex. *Chemical Geology* **150**, 85–103.

Maier, W. D., Barnes, S.-J. & Groves, D. I. (2013). The Bushveld Complex, South Africa: formation of platinum–palladium, chrome- and vanadium-rich layers via hydrodynamic sorting of a mobilized cumulate slurry in a large, relatively slowly cooling, subsiding magma chamber. *Mineralium Deposita* **48**, 1–56.

Maier, W. D., Barnes, S.-J. & Karykowski, B. T. (2016). A chilled margin of komatiite and Mg-rich basaltic andesite in the western Bushveld Complex, South Africa. *Contributions to Mineralogy and Petrology* **171**, 57.

Maier, W. D., Barnes, S.-J. & Van der Merwe, M. J. (2001). Platinum-group elements in the Pyroxenite Marker, Bushveld Complex: implications for the formation of the Main Zone. *South African Journal of Geology* **104**, 301–308.

Mangwegape, M., Roelofse, F., Mock, T. & Carlson, R. W. (2016). The Sr-isotopic stratigraphy of the Northern Limb of the Bushveld Complex, South Africa. *Journal of African Earth Sciences* **113**, 95–100.

Mathez, E. A. & Kent, A. J. R. (2007). Variable initial Pb isotopic compositions of rocks associated with the UG2 chromitite, eastern Bushveld Complex. *Geochimica et Cosmochimica Acta* **71**, 5514–5527.

Mathez, E. A. & Waight, T. E. (2003). Lead isotopic disequilibrium between sulfide and plagioclase in the Bushveld Complex and the chemical evolution of large layered intrusions. *Geochimica et Cosmochimica Acta* **67**, 1875–1888.

McDonough, W. F. & Sun, S. -s. (1995). The composition of the Earth. *Chemical Geology* **120**, 223–253.

Mitchell, A. A. (1986). The petrology, mineralogy and geochemistry of the Main Zone of the Bushveld Complex at Rustenburg Platinum Mines, Union Section. PhD thesis, Grahamstown, South Africa, Rhodes University.

Mitchell, A. A. (1990). The stratigraphy, petrography and mineralogy of the Main Zone of the northwestern Bushveld Complex. *South African Journal of Geology* **93**, 818–831.

Müller, W., Aerden, D. & Halliday, A. N. (2000). Isotopic dating of strain fringe increments: Duration and rates of deformation in shear zones. *Science* **288**, 2195–2198.

Müller, W., Kelley, S. P. & Villa, I. M. (2002). Dating fault-generated pseudotachylytes: comparison of 40Ar/39Ar stepwise-heating, laser-ablation and Rb–Sr microsampling analyses. *Contributions to Mineralogy and Petrology* **144**, 57–77.

Nebel, O., Scherer, E. E. & Mezger, K. (2011). Evaluation of the [87]Rb decay constant by age comparison against the U–Pb system. *Earth and Planetary Science Letters* **301**, 1–8.

Olszak-Humienik, M. & Jablonski, M. (2014). Thermal behavior of natural dolomite. *Journal of Thermal Analysis and Calorimetry* **119**, 2239–2248.

Phinney, W. C. (1992). Partition coefficients for iron between plagioclase and basalt as a function of oxygen fugacity: Implications for Archean and lunar anorthosites. *Geochimica et Cosmochimica Acta* **56**, 1885–1895.

Prevec, S. A., Ashwal, L. D. & Mkaza, M. S. (2005). Mineral disequilibrium in the Merensky Reef, western Bushveld Complex, South Africa: new Sm–Nd isotopic evidence. *Contributions to Mineralogy and Petrology* **149**, 306–315.

Pronost, J., Harris, C., & Pin, C. (2008). Relationship between footwall composition, crustal contamination, and fluid–rock interaction in the Platreef, Bushveld Complex, South Africa. *Mineralium Deposita* **43**, 825–848.

Ramos, F. C., Wolff, J. A. & Tollstrup, D. L. (2004). Measuring $^{87}Sr/^{86}Sr$ variations in minerals and groundmass from basalts using LA-MC-ICPMS. *Chemical Geology* **211**, 135–158.

Ramos, F. C., Wolff, J. A. & Tollstrup, D. L. (2005). Sr isotope disequilibrium in Columbia River flood basalts: Evidence for rapid shallow-level open-system processes. *Geology* **33**, 457–460.

Rankenburg, K., Lassiter, J. C. & Brey, G. (2004). Origin of megacrysts in volcanic rocks of the Cameroon volcanic chain – constraints on magma genesis and crustal contamination. *Contributions to Mineralogy and Petrology* **147**, 129–144.

Reid, D. L. & Basson, I. J. (2002). Iron-rich ultramafic pegmatite replacement bodies within the Upper Critical Zone, Rustenburg Layered Suite, Northam Platinum Mine, South Africa. *Mineralogical Magazine* **66**, 895–914.

Roelofse, F. (2010). Constraints on the magmatic evolution of the Lower Main Zone and Platreef on the northern limb of the Bushveld Complex as inferred from the Moordkopje drill core. PhD thesis, Johannesburg, South Africa, University of Witwatersrand.

Roelofse, F. & Ashwal, L. D. (2012). The lower Main Zone in the northern limb of the Bushveld Complex- a >1.3 km thick sequence of intruded and variably contaminated crystal mushes. *Journal of Petrology* **53**, 1449–1476.

Roelofse, F., Ashwal, L. D. & Romer, R. L. (2015). Multiple, isotopically heterogeneous plagioclase populations in the Bushveld Complex suggest mush intrusion. *Chemie der Erde - Geochemistry* **75**, 357–364.

Scoates, J. S. & Wall, C. J. (2015). Geochronology of layered intrusions. In: Charlier, B., Namur, O., Latypov, R. & Tegner, C. (eds) *Layered Intrusions*. Springer, 3–74.

Scoon, R. N. & Mitchell, A. A. (1994). Discordant iron-rich ultramafic pegmatites in the Bushveld Complex and their relationship to iron-rich intercumulus and residual liquids. *Journal of Petrology* **35**, 881–917.

Seabrook, C. L. (2005). The Upper Critical and Lower Main Zones of the eastern Bushveld Complex. PhD thesis, Johannesburg, South Africa, University of Witwatersrand.

Seabrook, C. L., Cawthorn, R. G. & Kruger, F. J. (2005). The Merensky Reef, Bushveld Complex: mixing of minerals not mixing of magmas. *Economic Geology* **100**, 1191–1206.

Sharpe, M. R. (1981). The chronology of magma influxes to the eastern compartment of the Bushveld Complex as exemplified by its marginal border groups. *Journal of the Geological Society* **138**, 307–326.

Sharpe, M. R. (1985). Strontium isotope evidence for preserved density stratification in the main zone of the Bushveld Complex, South Africa. *Nature* **316**, 119–126.

Spandler, C. & Pirard, C. (2013). Element recycling from subducting slabs to arc crust: A review. *Lithos* **170–171**, 208–223.

Swart, Q. D. (1999). Carbonate rocks of the Paleoproterozoic Pretoria and Postmasburg Groups, Transvaal Supergroup. MSc thesis, Johannesburg, South Africa, Rand Afrikaans University.

Teigler, B. (1990). Mineralogy, petrology and geochemistry of the Lower and Lower Critical Zones, northwestern Bushveld Complex. PhD thesis, Grahamstown, South Africa, Rhodes University.

Tepley, F. J. & Davidson, J. P. (2003). Mineral-scale Sr-isotope constraints on magma evolution and chamber dynamics in the Rum layered intrusion, Scotland. *Contributions to Mineralogy and Petrology* **145**, 628–641.

VanTongeren, J. A. & Mathez, E. A. (2013). Incoming magma composition and style of recharge below the Pyroxenite Marker, eastern Bushveld Complex, South Africa. *Journal of Petrology* **54**, 1585–1605.

Veizer, J., Clayton, R. N. & Hinton, R. W. (1992). Geochemistry of Precambrian carbonates: IV. Early Paleoproterozoic (2.25 ± 0.25 Ga) seawater. *Geochimica et Cosmochimica Acta* **56**, 875–885.

Walraven, F. & Martini, J. (1995). Zircon Pb-evaporation age determinations for the Oak Tree Formation, Chuniespoort Group, Transvaal Sequence; implications for Transvaal-Griqualand West basin correlations. *South African Journal of Geology* **98**, 58–67.

Weaver, B. L. & Tarney, J. (1980). Rare earth geochemistry of Lewisian granulite-facies gneisses, northwest Scotland: Implications for the petrogenesis of the Archaean lower continental crust. *Earth and Planetary Science Letters* **51**, 279–296.

Wei, X., Xu, Y.-G., Zhang, C.-L., Zhao, J.-X. & Feng, Y.-X. (2014). Petrology and Sr–Nd isotopic disequilibrium of the Xiaohaizi intrusion, NW China: Genesis of layered intrusions in the Tarim Large Igneous Province. *Journal of Petrology* **55**, 2567–2598.

Wenzel, T., Baumgartner, L. P., Brügmann, G. E., Konnikov, E. G. & Kislov, E. V. (2002). Partial melting and assimilation of dolomitic xenoliths by mafic magma: the Ioko-Dovyren Intrusion (North Baikal Region, Russia). *Journal of Petrology* **43**, 2049–2074.

Wilson, A. H. (2012). A chill sequence to the Bushveld Complex: Insight into the first stage of emplacement and implications for the parental magmas. *Journal of Petrology* **53**, 1123–1168.

Wilson, A. H. & Chunnett, G. (2006). Trace element and platinum group element distributions and the genesis of the Merensky Reef, western Bushveld Complex, South Africa. *Journal of Petrology* **47**, 2369–2403.

Yang, S.-H., Maier, W. D., Lahaye, Y. & O'Brien, H. (2013). Strontium isotope disequilibrium of plagioclase in the Upper Critical Zone of the Bushveld Complex: evidence for mixing of crystal slurries. *Contributions to Mineralogy and Petrology* **166**, 959–974.

Zeh, A., Ovtcharova, M., Wilson, A. H. & Schaltegger, U. (2015). The Bushveld Complex was emplaced and cooled in less than one million years – results of zirconology, and geotectonic implications. *Earth and Planetary Science Letters* **418**, 103–114.

FIGURES AND TABLES

Figure 1: Simplified geological map of the Bushveld Complex showing the location of the Bellevue drill core and Union Section. Abbreviations: TML = Thabazimbi-Murchison Lineament. Modified after Maier *et al.* (2013).

Figure 2: Measured *in situ* Sr isotope compositions of the in-house standard MIR a. The error bar represents 2σ.

Figure 3: Plot of weighted average *in situ* ^{87}Sr/^{86}Sr$_i$ ratios together with the average anorthite contents, the average FeO concentrations in plagioclase, εNd values from Maier *et al.* (2001, 2013) and chondrite-normalised Ce/Sm ratios against stratigraphic height. Trace element data were taken from Maier *et al.* (2013). Normalisation values were taken from McDonough & Sun (1995). Abbreviations: UZ = Upper Zone; MZ = Main Zone; UCZ = Upper Critical Zone; LCZ = Lower Critical Zone; LZ = Lower Zone.

Figure 4: Intra-sample *in situ* Sr isotope variation coupled with anorthite contents. a) Lower Zone. b) Critical Zone. c) Main Zone. d) Upper Zone. Abbreviations: C = cumulus; I = intercumulus.

Figure 5: Plot of weighted average *in situ* and whole rock ^{87}Sr/^{86}Sr$_i$ ratios together with average anorthite contents, Mg# in orthopyroxene, whole rock Mg# and chondrite-normalised Ce/Sm ratios for the Lower Zone. The standard deviation is represented by the error bar. Whole rock data and mineral compositions were taken from Teigler (1990). Trace element data were taken from Maier *et al.* (2013). *In situ* Sr isotopic data for the chill sequence (Chill

seq.) were taken from Maier *et al.* (2016). Normalisation values were taken from McDonough & Sun (1995).

Figure 6: Plot of weighted average *in situ* $^{87}Sr/^{86}Sr_i$ ratios vs. anorthite content for samples from the Lower Zone (LZ) and the Lower Critical Zone (LCZ).

Figure 7: Plot of weighted average *in situ* and whole rock $^{87}Sr/^{86}Sr_i$ ratios together with average anorthite contents, Mg# in orthopyroxene, whole rock Mg# and chondrite-normalised Ce/Sm ratios for the Lower and Upper Critical Zone. The standard deviation is represented by the error bar. Whole rock data and mineral compositions were taken from Teigler (1990) and De Klerk (1991), respectively. Trace element data were taken from Maier *et al.* (2013). Normalisation values were taken from McDonough & Sun (1995).

Figure 8: Plot of weighted average *in situ* $^{87}Sr/^{86}Sr_i$ ratios vs. chondrite-normalised Ce/Sm ratios for samples from all zones of the Bushveld Complex. Trace element data were taken from Maier *et al.* (2013). Normalisation values were taken from McDonough & Sun (1995).

Figure 9: Plot of weighted average *in situ* and whole rock $^{87}Sr/^{86}Sr_i$ ratios together with average anorthite contents, Mg# in orthopyroxene, whole rock Mg# and chondrite-normalised Ce/Sm ratios for the Main Zone. The standard deviation is represented by the error bar. Whole rock data and mineral compositions were taken from Mitchell (1986). Trace element data were taken from Maier *et al.* (2013). Normalisation values were taken from McDonough & Sun (1995).

Figure 10: Plot of weighted average *in situ* and whole rock $^{87}Sr/^{86}Sr_i$ ratios together with average anorthite contents, Mg# in orthopyroxene, whole rock Mg# and chondrite-normalised Ce/Sm ratios for the Upper Zone. The standard deviation is represented by the error bar. Sr isotope data from the northern limb were taken from Mangwegape *et al.* (2016). Whole rock data and mineral compositions were taken from Barnes *et al.* (2004) and Ashwal *et al.* (2005), respectively. Note that the whole rock $^{87}Sr/^{86}Sr_i$ ratios shown for comparison are not from the Bellevue drill core, but from the western limb analysed by Kruger *et al.* (1987). Trace element data were taken from Maier *et al.* (2013). Normalisation values were taken from McDonough & Sun (1995).

Figure 11: Plot of anorthite contents against weighted average *in situ* $^{87}Sr/^{86}Sr_i$ ratios for different samples from the Upper Critical Zone. Data for the squares were taken from Yang *et al.* (2013). Data for the base of the Main Zone were taken from Seabrook *et al.* (2005). Data for the lower Main Zone were taken from Roelofse (2010). The standard deviation is represented by the error bar. Abbreviations: MZ = Main Zone; UCZ = Upper Critical Zone; BCU = Bastard Cyclic Unit; MCU = Merensky Cyclic Unit; UG1 = Upper Group 1 chromite layer; FW = footwall. Symbols marked with a "C" are samples with cumulus plagioclase.

Figure 12: Plot of anorthite contents against weighted average *in situ* $^{87}Sr/^{86}Sr_i$ ratios for different samples from the Main Zone. The standard deviation is represented by the error bar. Data for the base of the MZ and the northern limb MZ were taken from Seabrook (2005) and Mangwegape *et al.* (2016), respectively. Abbreviations: MZ = Main Zone; UCZ = Upper Critical Zone; E-BV = Eastern limb of the Bushveld Complex; N-BV = Northern limb of the Bushveld Complex.

Figure 13: Plot of the *in situ* $^{87}Sr/^{86}Sr_i$ ratios standard deviation (2σ) against stratigraphic height. Data for the Upper Zone and Upper Critical Zone (grey symbols) were taken from Mangwegape *et al.* (2016) and Yang *et al.* (2013), respectively. Abbreviations: UCZ = Upper Critical Zone; LCZ = Lower Critical Zone; LZ = Lower Zone.
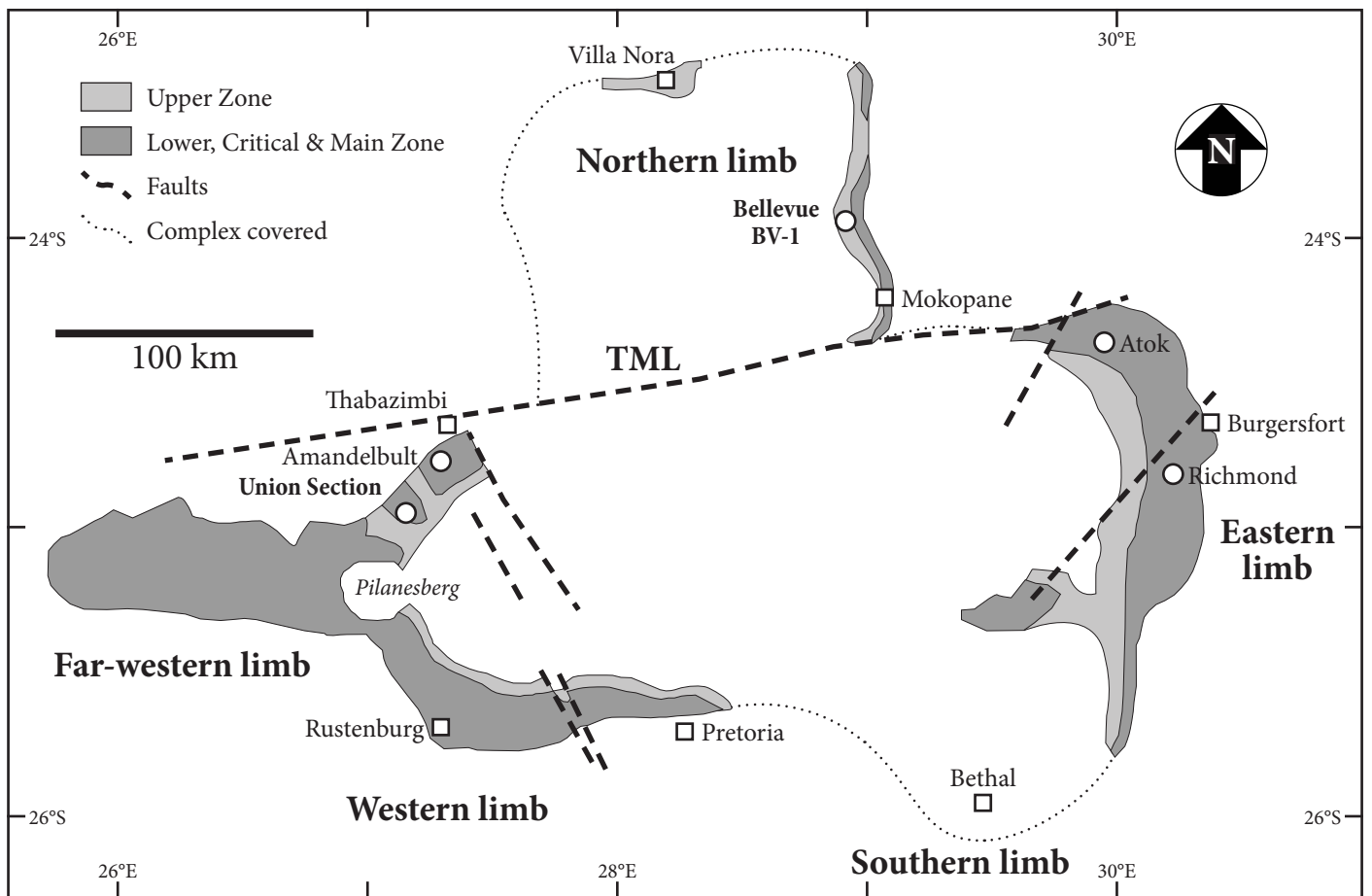
Figure 14: Elemental maps showing the variation of Na in plagioclase. a) Interstitial plagioclase from the Lower Zone in sample NG2-762.27. b) Interstitial plagioclase from the Lower Zone in sample NG2-762.27. c) Zoned cumulus plagioclase from the Main Zone in sample A168.

Figure 15: Model for the observed regional variations of $^{87}Sr/^{86}Sr_i$ ratios among MCU profiles from different areas of the Bushveld Complex. a) Regionally non-uniform mixing between isotopically distinct MZ and CZ magma. b) Crystallisation of a proto-cumulate that reflects the different degrees in mixing. c) After the mobilisation of the proto-cumulate in a crystal slurry and associated density sorting, the variations in $^{87}Sr/^{86}Sr_i$ ratios are still present across individual continuous layers. Rectangles: plagioclase; squares: pyroxene; circles = chromite. Abbreviations: MZ = Main Zone; CZ = Critical Zone; MCU = Merensky Cyclic Unit.
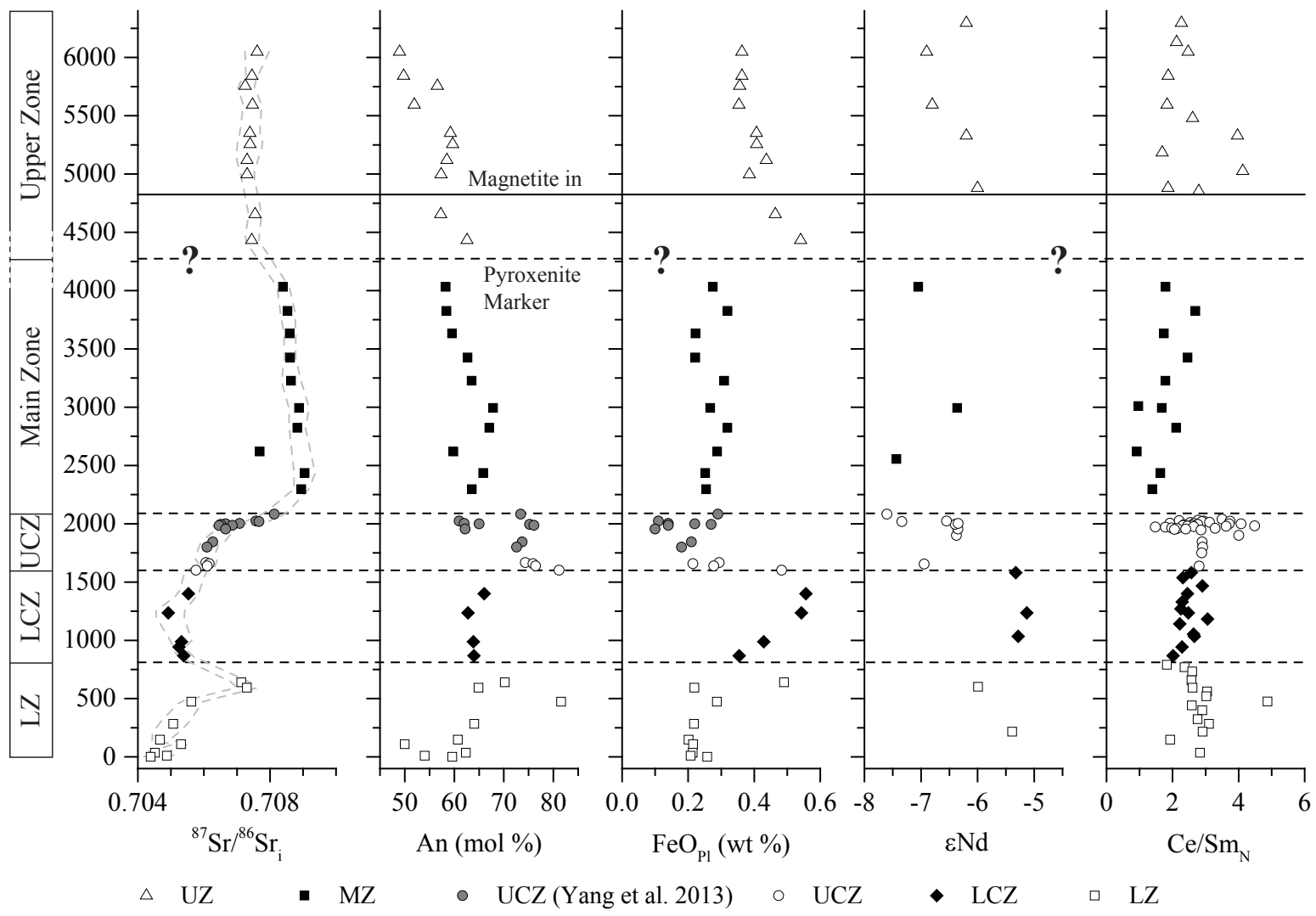
Figure 16: Chondrite-normalised rare earth element (REE) pattern for sample A238 from the Main Zone. The average MZ gabbronorite REE pattern and the range of iron-rich ultramafic pegmatites (IRUP) are shown for comparison. Whole rock data for MZ and UCZ IRUP samples were taken from Barnes *et al.* (2004) and Reid & Basson (2002), respectively. Normalisation values were taken from McDonough & Sun (1995). Abbreviations: MZ = Main Zone; UCZ = Upper Critical Zone.
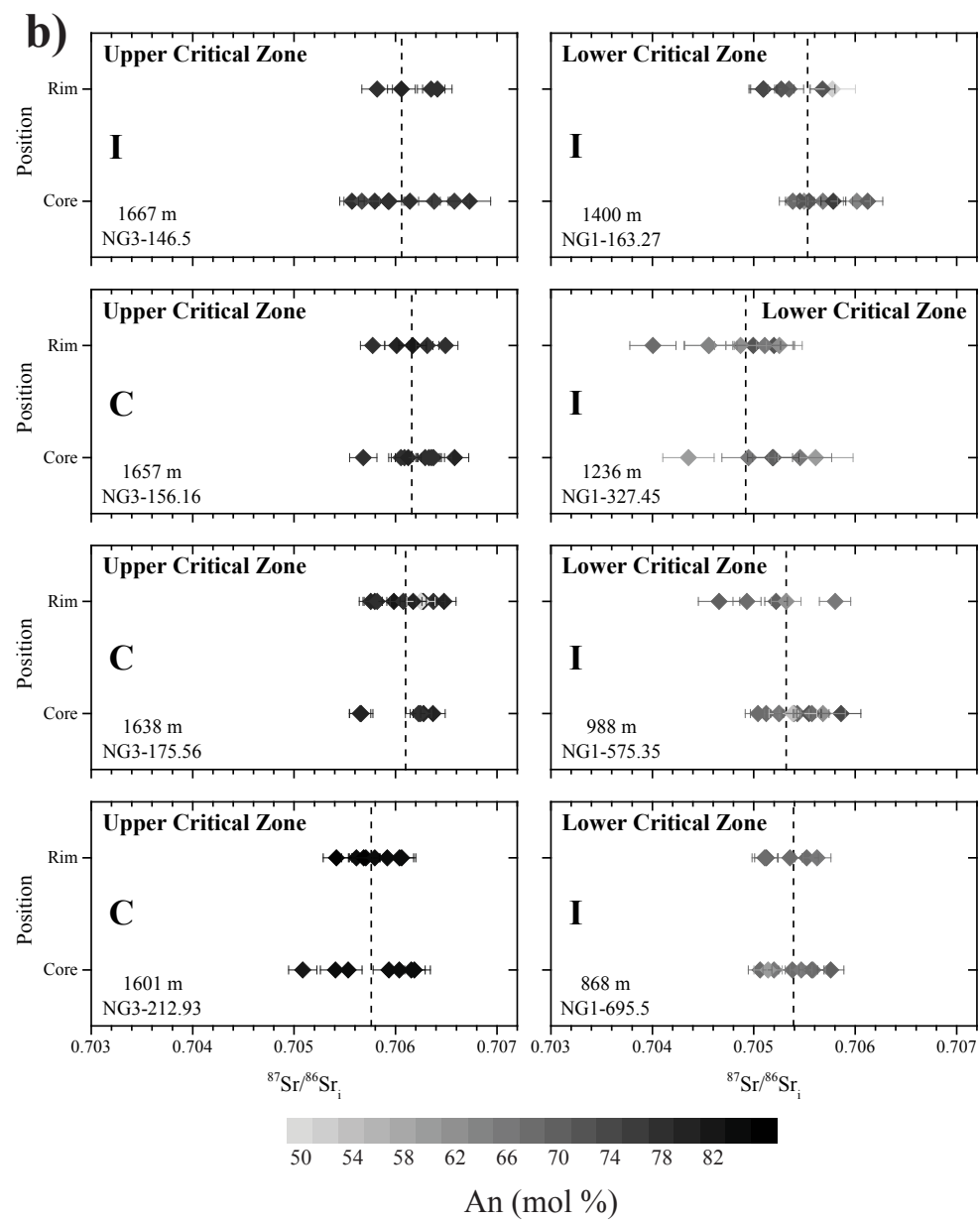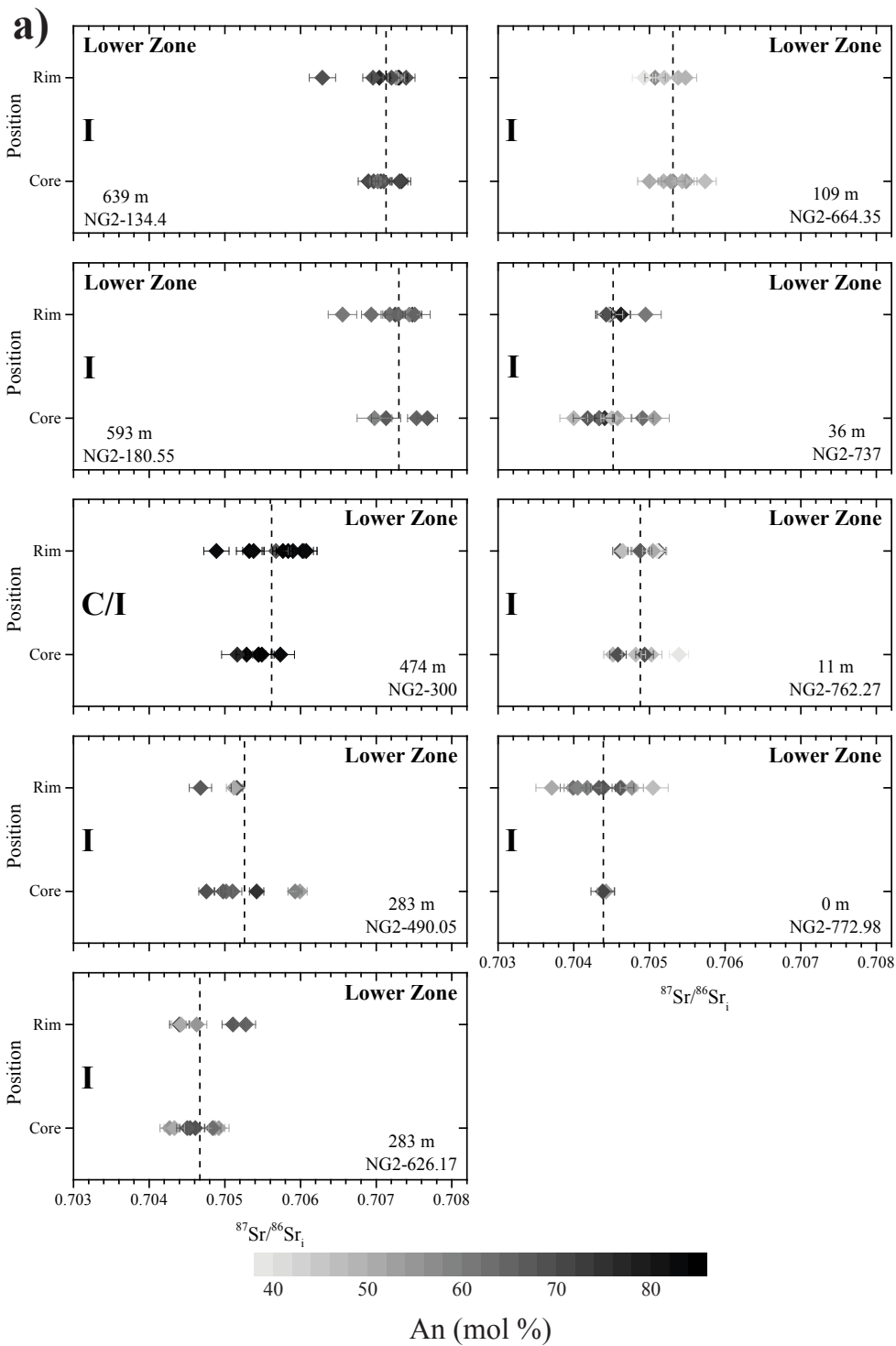
Table 1: Weighted average *in situ* Sr isotope compositions, anorthite contents and FeO concentrations of plagioclase, Union Section, western Bushveld Complex. Initial $^{87}Sr/^{86}Sr_i$ is recalculated to 2,055 Ma (Zeh *et al.*, 2015). The number of analyses per sample is given as "n"
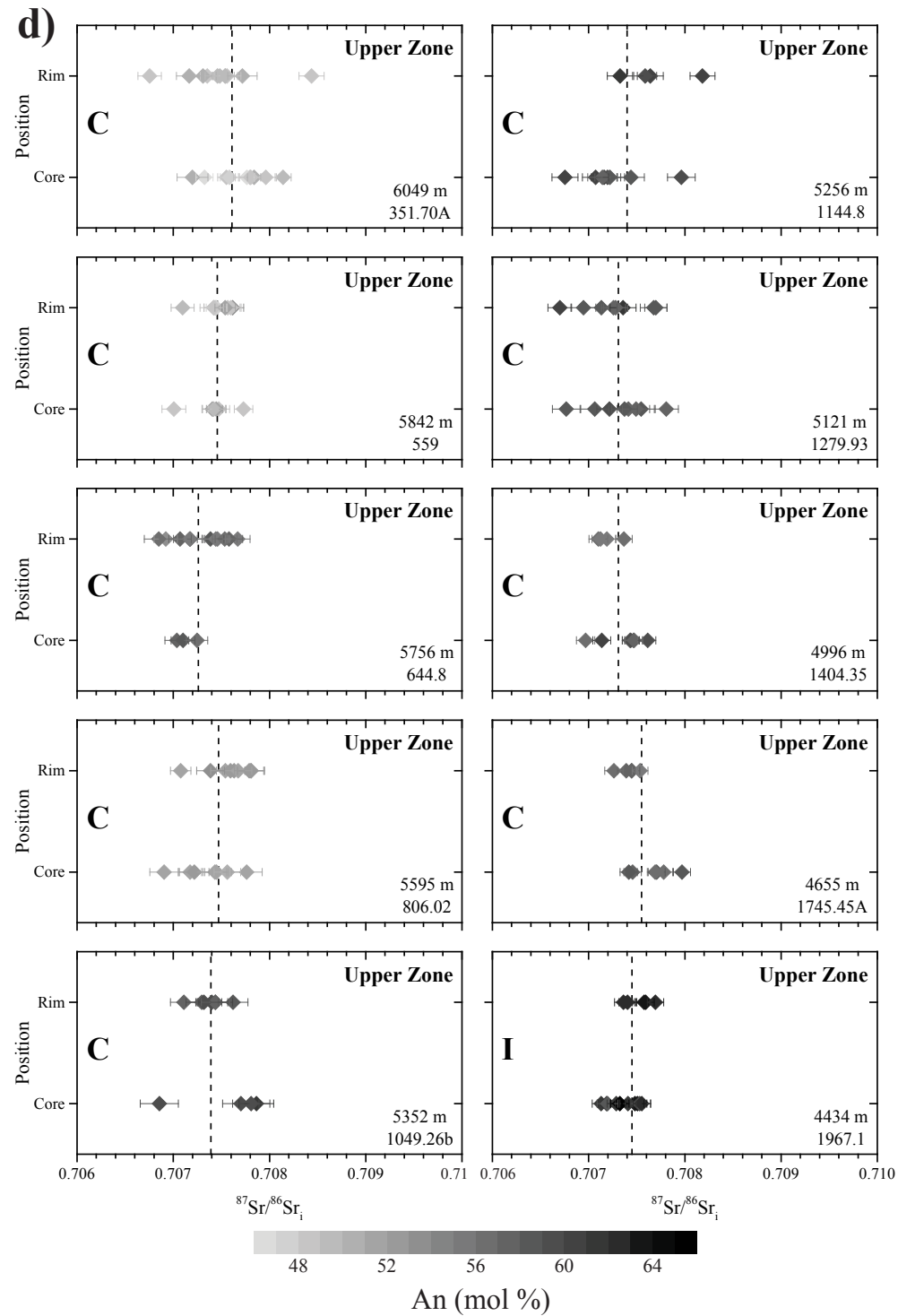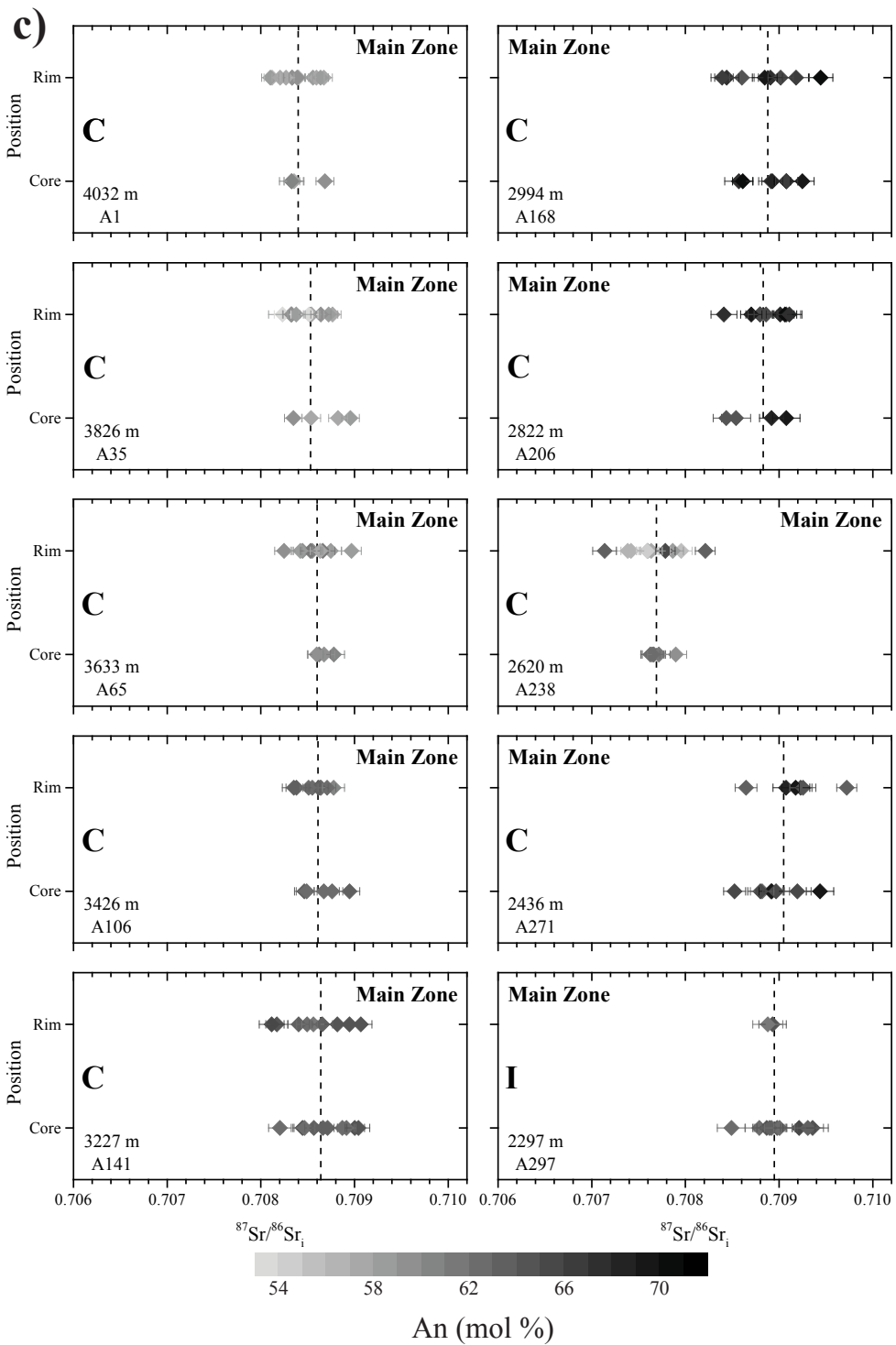
Table 2: Calculated Sr_i of pyroxene from sample A1 based on mineral mode, Sr concentrations, whole rock Sr data and the *in situ* Sr_i ratio of plagioclase
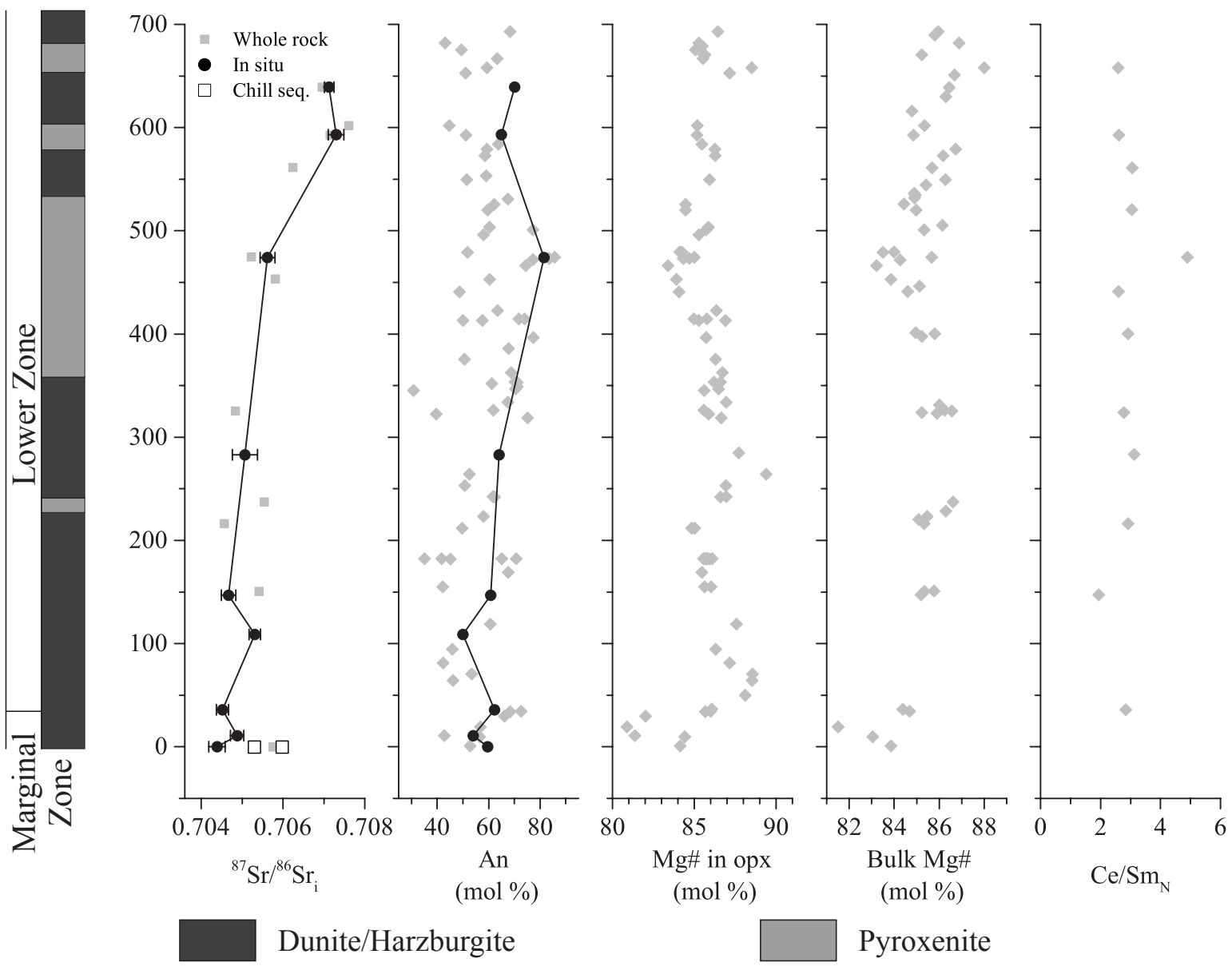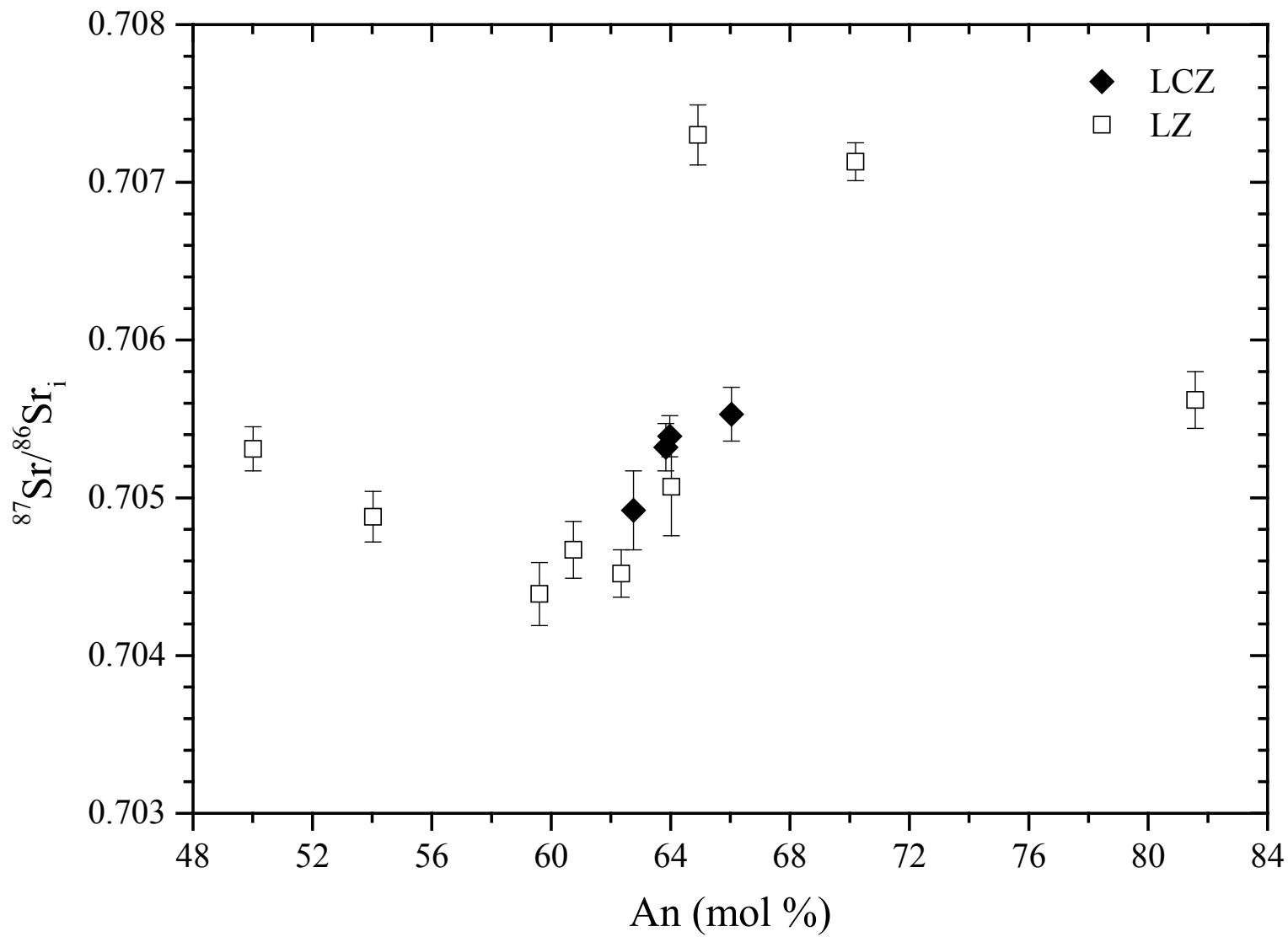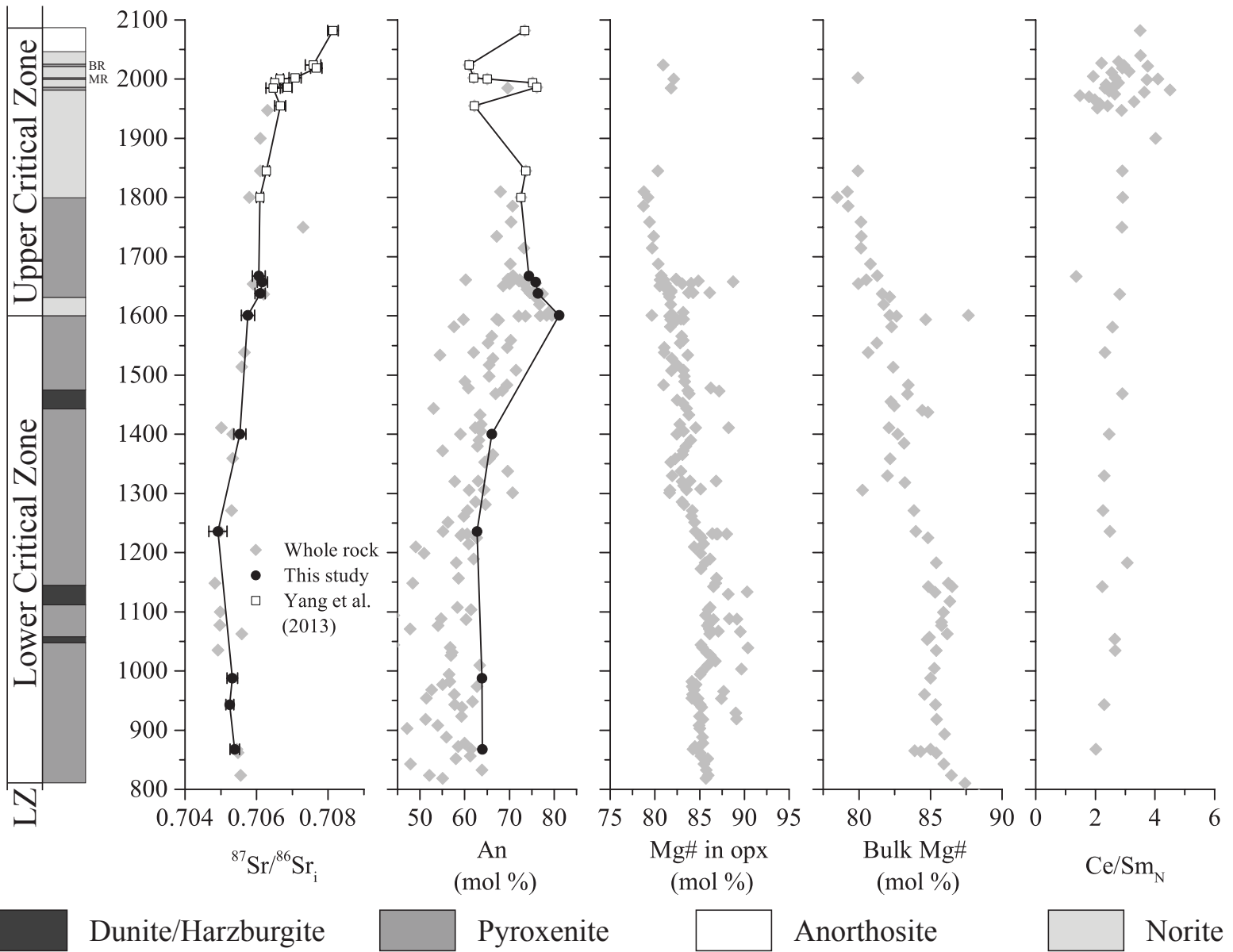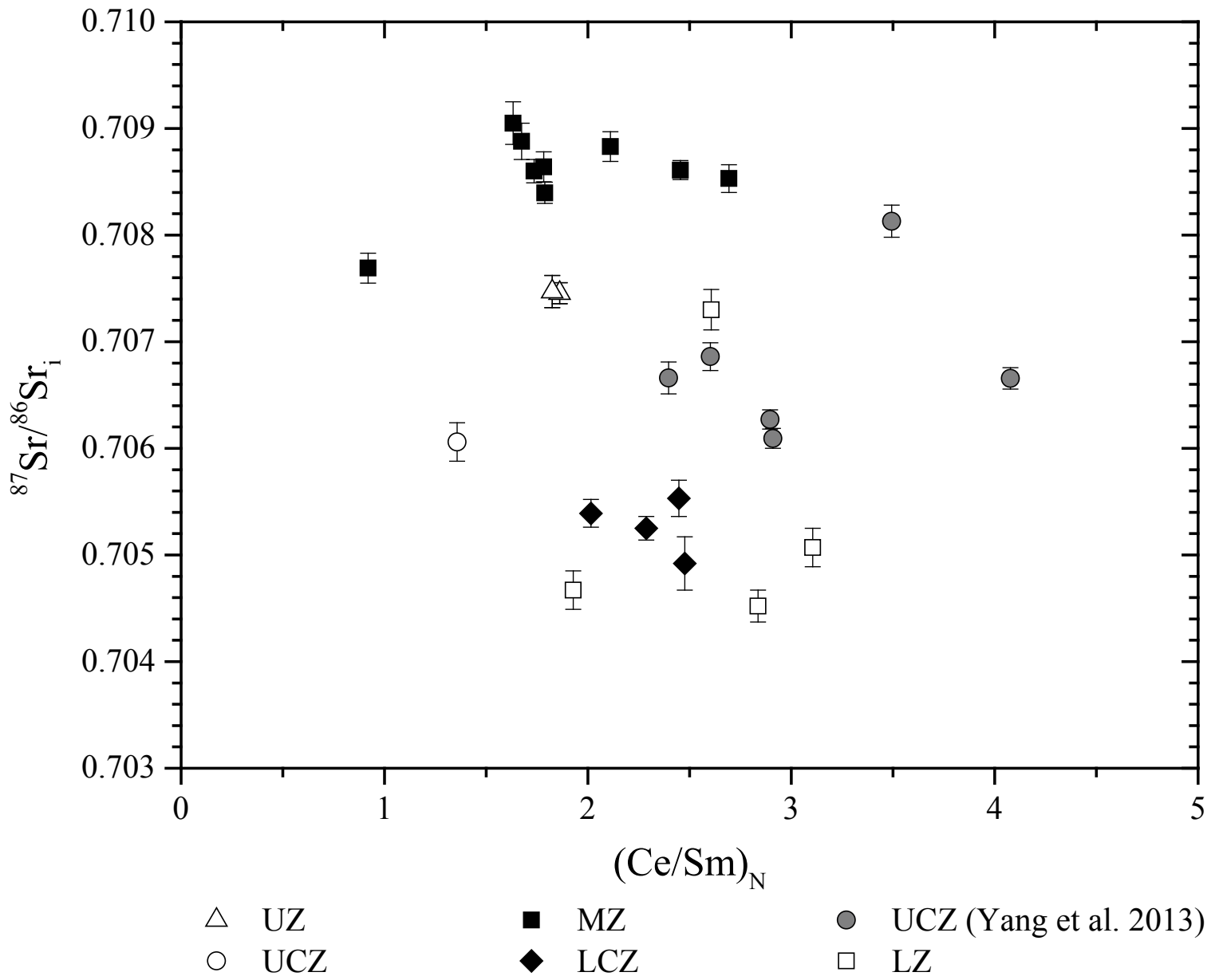
Reference value: 0.703096 ± 0.000070

(2σ, Rankenburg *et al.*, 2004)

Mean average $^{87}Sr/^{86}Sr$ ratio: 0.703106 ± 0.000090 (2σ, n = 85)

Number of analyses

$^{87}Sr/^{86}Sr$

a)

Lower Zone — 639 m, NG2-134.4 (I)

Lower Zone — 109 m, NG2-664.35 (I)

Lower Zone — 593 m, NG2-180.55 (I)

Lower Zone — 36 m, NG2-737 (I)

Lower Zone — 474 m, NG2-300 (C/I)

Lower Zone — 11 m, NG2-762.27 (I)

Lower Zone — 283 m, NG2-490.05 (I)

Lower Zone — 0 m, NG2-772.98 (I)

Lower Zone — 283 m, NG2-626.17 (I)

$^{87}Sr/^{86}Sr_i$

An (mol %): 40 50 60 70 80

b)

Upper Critical Zone — 1667 m, NG3-146.5 (I)

Lower Critical Zone — 1400 m, NG1-163.27 (I)

Upper Critical Zone — 1657 m, NG3-156.16 (C)

Lower Critical Zone — 1236 m, NG1-327.45 (I)

Upper Critical Zone — 1638 m, NG3-175.56 (C)

Lower Critical Zone — 988 m, NG1-575.35 (I)

Upper Critical Zone — 1601 m, NG3-212.93 (C)

Lower Critical Zone — 868 m, NG1-695.5 (I)

$^{87}Sr/^{86}Sr_i$

An (mol %): 50 54 58 62 66 70 74 78 82

Whole rock
In situ
Chill seq.

$^{87}Sr/^{86}Sr_i$

An
(mol %)

Mg# in opx
(mol %)

Bulk Mg#
(mol %)

Ce/Sm$_N$

Lower Zone

Marginal
Zone

Dunite/Harzburgite

Pyroxenite

Whole rock
This study
Yang et al.
(2013)

Upper Critical Zone

Lower Critical Zone

LZ

BR
MR

2100
2000
1900
1800
1700
1600
1500
1400
1300
1200
1100
1000
900
800

0.704   0.706   0.708
$^{87}Sr/^{86}Sr_i$

50   60   70   80
An
(mol %)

75   80   85   90   95
Mg# in opx
(mol %)

80   85   90
Bulk Mg#
(mol %)

0   2   4   6
Ce/Sm$_N$

Dunite/Harzburgite   Pyroxenite   Anorthosite   Norite

UZ

Main Zone

UCZ

4400
4200
4000
3800
3600
3400
3200
3000
2800
2600
2400
2200
2000
1800

0.70769

Whole rock
In situ

0.708 0.709
$^{87}Sr/^{86}Sr_i$

60 70
An
(mol %)

60 70 80
Mg# in opx
(mol %)

60 70 80
Bulk Mg#
(mol %)

0 2 4 6
Ce/Sm_N

Gabbronorite   Pyroxenite   Anorthosite   Mafic pegmatite

△	UZ	▲	UZ (Mangwegape et al. 2016)
■	MZ		
○	UCZ	●	UCZ (Yang et al. 2013)
◆	LCZ	□	LZ
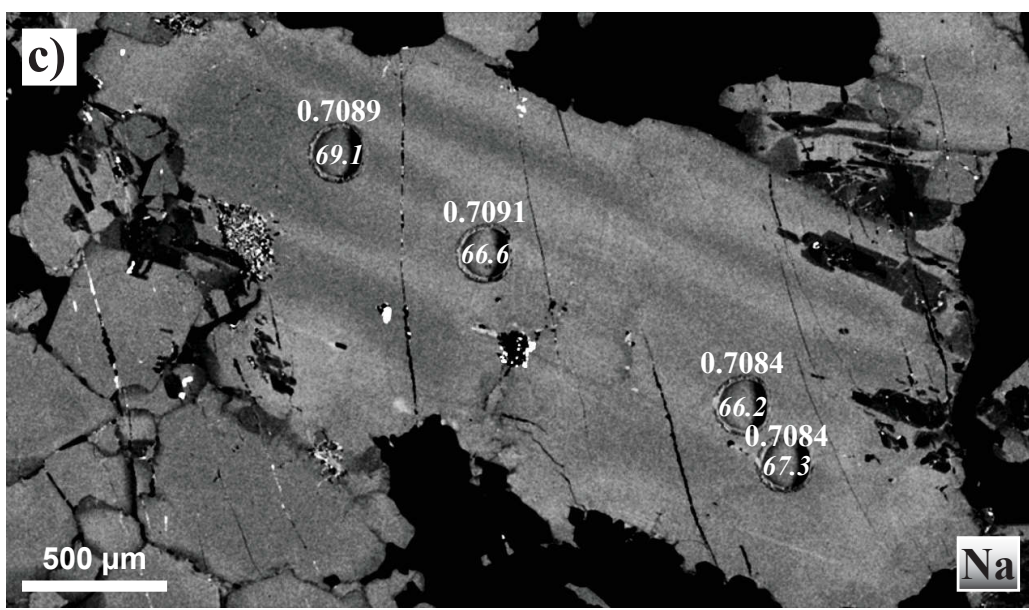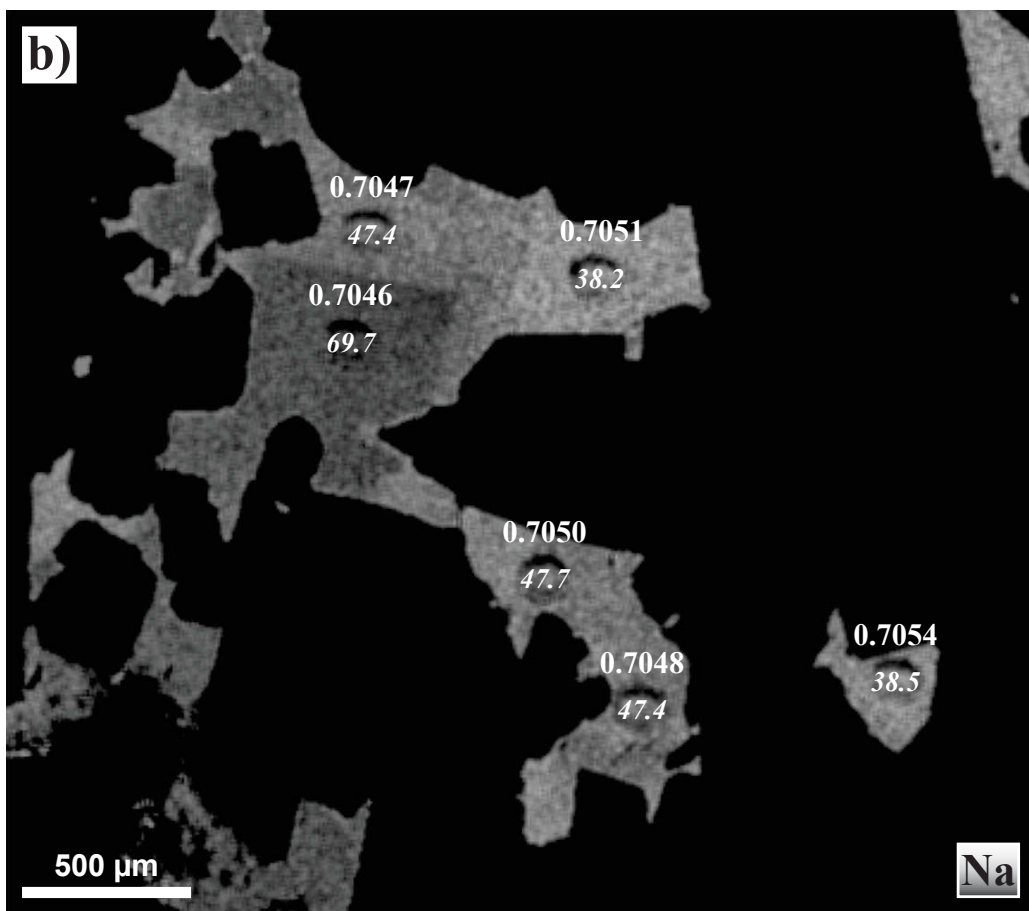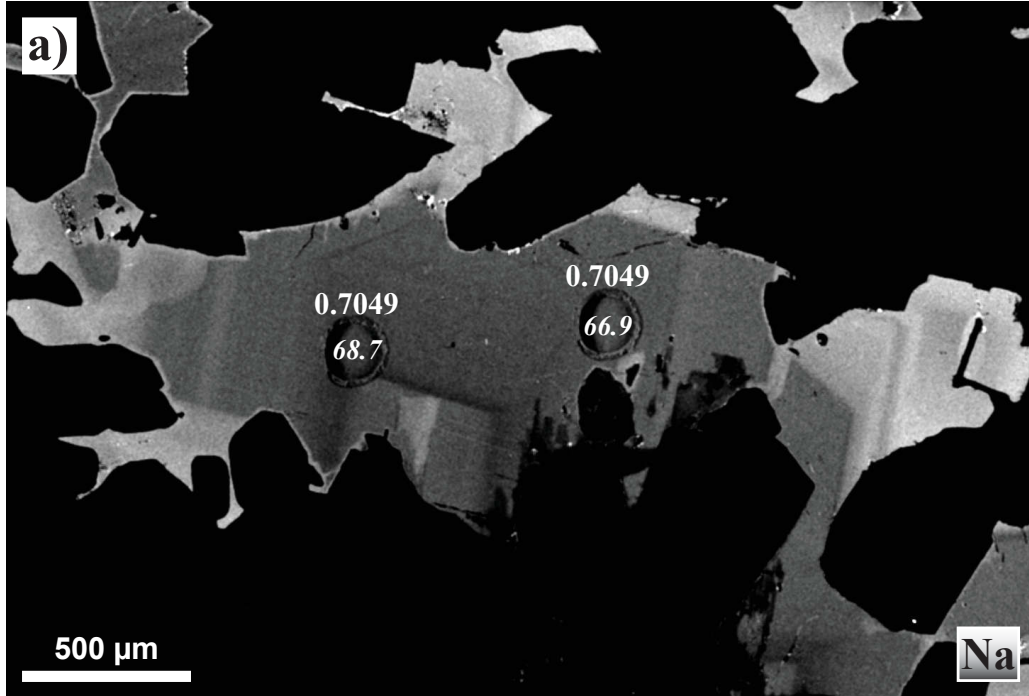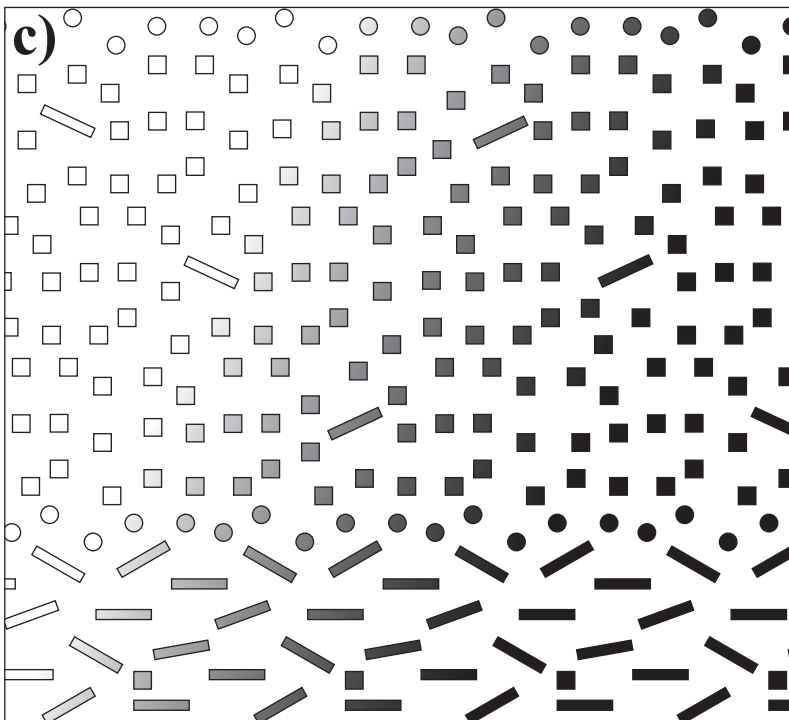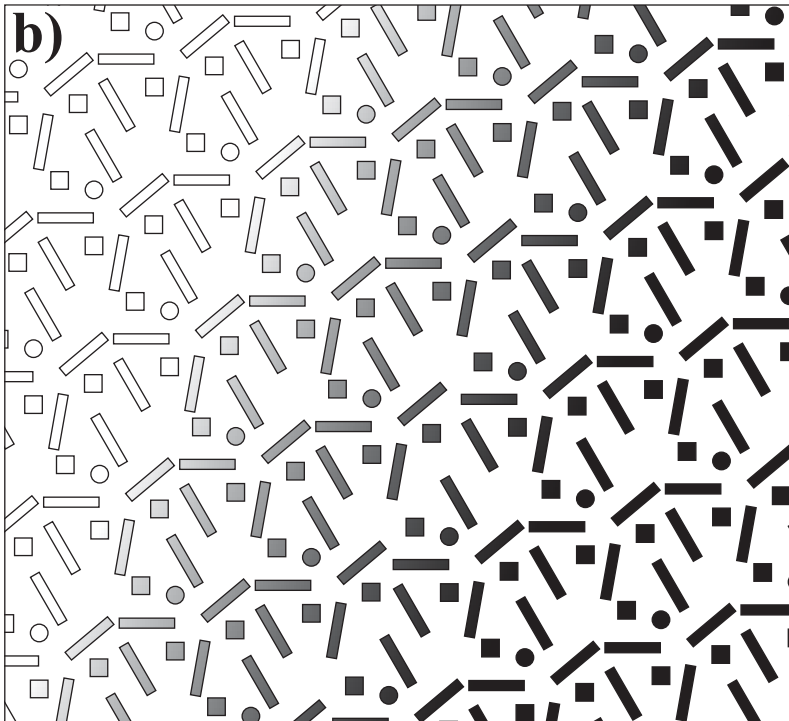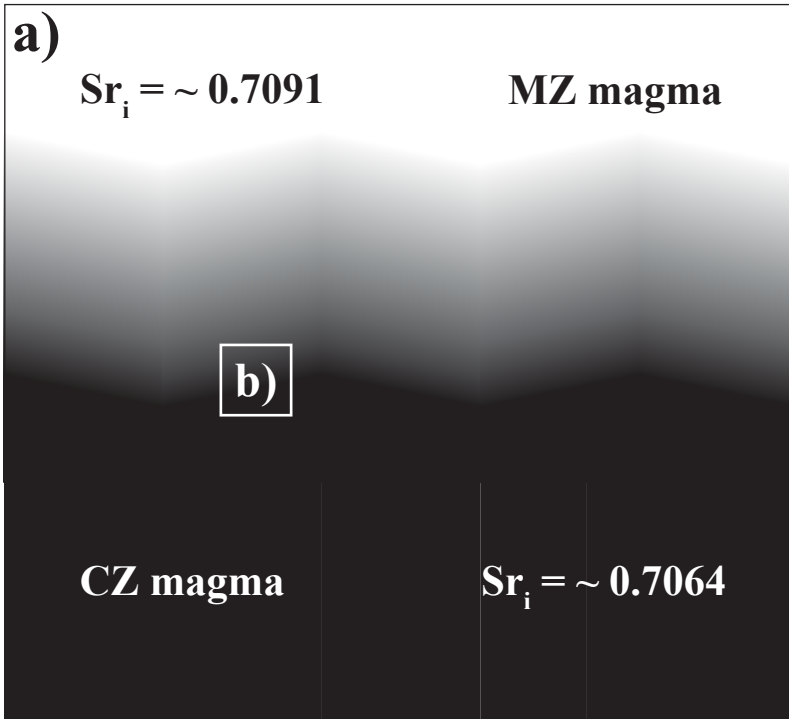
a) 0.7049 68.7 0.7049 66.9 500 µm Na

b) 0.7047 47.4 0.7051 38.2 0.7046 69.7 0.7050 47.7 0.7048 47.4 0.7054 38.5 500 µm Na

c) 0.7089 69.1 0.7091 66.6 0.7084 66.2 0.7084 67.3 500 µm Na

a) $Sr_i = \sim 0.7091$ MZ magma

b)

CZ magma $Sr_i = \sim 0.7064$

b)

c)

Table 1. Weighted average *in situ* Sr isotope compositions, anorthite contents and FeO concentrations of plagioclase, Union Section, western Bushveld Complex. Initial $^{87}Sr/^{86}Sr_i$ is recalculated to 2,055 Ma (Zeh *et al*. 2015). The number of analyses per sample is given as "n"
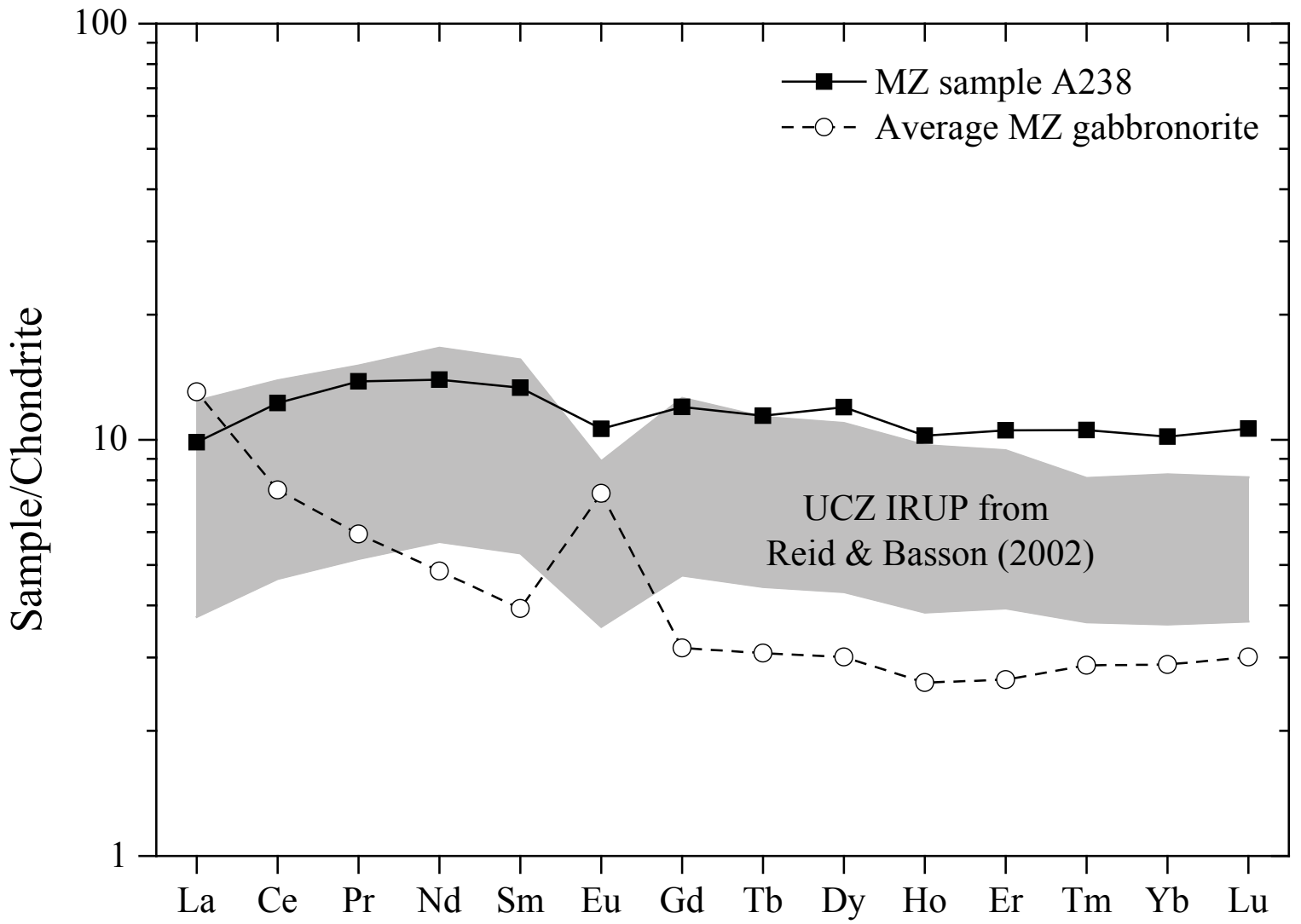
Sample	Height (m)	Unit	Rock	$^{87}Sr/^{86}Sr_i$	2σ	An	FeO (wt %)	n
351.70A	6049	UZ	Mt	0.70761	0.00015	48.9	0.36	21
559	5842	UZ	Mt-G	0.70745	0.00010	49.8	0.36	15
644.8	5756	UZ	Mt	0.70725	0.00014	56.6	0.36	14
806.02	5595	UZ	Mt-G	0.70747	0.00015	51.9	0.35	16
1049.26b	5352	UZ	Mt-G	0.70739	0.00018	59.2	0.41	12
1144.8	5256	UZ	Mt-G	0.70740	0.00026	59.7	0.41	12
1279.93	5121	UZ	Mt-G	0.70731	0.00017	58.5	0.44	16
1404.35	4996	UZ	Mt-G	0.70731	0.00012	57.3	0.39	12
1745.45A	4655	UZ	G	0.70755	0.00012	57.3	0.46	12
1967.1	4434	UZ	G	0.70745	0.00011	62.6	0.54	16
A1	4032	MZ	GN	0.70840	0.00010	58.3	0.28	16
A35	3826	MZ	GN	0.70853	0.00013	58.4	0.32	14
A65	3633	MZ	GN	0.70860	0.00011	59.6	0.22	13
A106	3426	MZ	GN	0.70861	0.00009	62.7	0.22	14
A141	3227	MZ	GN	0.70864	0.00014	63.5	0.31	19
A168	2994	MZ	GN	0.70888	0.00017	67.8	0.27	15
A206	2822	MZ	GN	0.70883	0.00014	67.1	0.32	13
A238	2620	MZ	GN	0.70769	0.00014	59.8	0.29	15
A271	2436	MZ	GN	0.70905	0.00020	65.8	0.25	14
A297	2297	MZ	Px	0.70895	0.00014	63.6	0.25	13
NG3-146.5	1667	UCZ	Px	0.70606	0.00018	74.4	0.29	15
NG3-156.16	1657	UCZ	An	0.70616	0.00014	75.9	0.21	15
NG3-175.56	1638	UCZ	N	0.70610	0.00014	76.4	0.28	17
NG3-212.93	1601	UCZ	An	0.70576	0.00018	81.1	0.48	15
NG1-163.27	1400	LCZ	Px	0.70553	0.00017	66.0	0.56	15
NG1-327.45	1236	LCZ	Px	0.70492	0.00025	62.8	0.54	14
NG1-575.35	988	LCZ	Px	0.70532	0.00015	63.8	0.43	16
NG1-695.5	868	LCZ	Px	0.70539	0.00013	64.0	0.35	14
NG2-134.4	639	LZ	Dun	0.70713	0.00012	70.2	0.49	15
NG2-180.55	593	LZ	Px	0.70730	0.00019	64.9	0.22	12
NG2-300	474	LZ	Px	0.70562	0.00018	81.6	0.29	16
NG2-490.05	283	LZ	Hz	0.70507	0.00018	64.0	0.22	10
NG2-626.17	147	LZ	Ol-Px	0.70467	0.00018	60.7	0.20	13
NG2-664.35	109	LZ	Hz	0.70531	0.00014	50.0	0.22	12
NG2-737	36	LZ	N	0.70452	0.00015	62.3	0.21	14
NG2-762.27	11	LZ	GN	0.70488	0.00016	54.0	0.21	13
NG2-772.98	0	LZ	GN	0.70439	0.00020	59.6	0.26	12

UZ = Upper Zone, MZ = Main Zone, UCZ = Upper Critical Zone, LCZ = Lower Critical Zone, LZ = Lower Zone

Mt = magnetitite, Mt-G = magnetitite-gabbro, G = Gabbro, GN = gabbronorite, N = norite,

A = anorthosite, Px = pyroxenite, Ol-Px = olivine-pyroxenite, Hz = harzburgite, Dun = dunite

Table 2. Calculated Sr_i of pyroxene from sample A1 based on mineral mode, Sr concentrations, whole rock Sr data and the *in situ* Sr_i ratio of plagioclase

Mineral	[1]Mode (vol %)	[2]Sr_{Min} (ppm)	*In situ* Sr_i	Calculated Sr_i
Plagioclase	65.4	365	0.70839	-
Orthopyroxene	24.4	9	-	0.69689
Clinopyroxene	10.2	27	-	
[*]**Whole rock Sr isotope composition of MZ sample A1: 0.70816**				

[1]Data from Mitchell (1986)

[2]Average Sr concentrations based on MZ mineral separates from Roelofse (2010)

	[1]Mode (vol %)	[2]Sr_{Min} (ppm)	*In situ* Sr_i	Calculated Sr_i